

## Article

# Research on Aerodynamic Test Validation and the Vector Force Control Method for an E-STOL Fan Wing Unmanned Aerial Vehicle

Siliang Du <sup>1,2,\*</sup>, Yi Zha <sup>1</sup> and Qijun Zhao <sup>2</sup>

<sup>1</sup> Unmanned Aerial Vehicles Research Institute, HuaiYin Institute of Technology, Huaian 223003, China; zy18136222322@163.com

<sup>2</sup> National Key Laboratory of Helicopter Aeromechanics, Nanjing University of Aeronautics and Astronautics, Nanjing 210016, China; zhaoqijun@nuaa.edu.cn

\* Correspondence: dusl\_aircraft@nuaa.edu.cn

**Abstract:** The concept of the Fan Wing, a novel aircraft vector-force-integrated device that combines a power unit with a fixed wing to generate distributed lift and thrust by creating a low-pressure vortex on the wing's surface, was studied. To investigate the unique propulsion mechanism of the Fan Wing, a Fan Wing test platform was developed, and experiments were conducted in a wind tunnel. At the same time, numerical simulations were established. In order to further improve the aerodynamic efficiency of the Fan Wing and decouple the control of lift and thrust, an improved scheme for the leading-edge structure of the Fan Wing was proposed, and a numerical analysis was conducted. A Fan Wing unmanned aerial vehicle (UAV) was designed and manufactured using the Fan Wing as the source of lift and thrust for the aircraft, and flight verification was conducted. The wind tunnel tests have proven that the main factors influencing the lift and thrust of the Fan Wing are rotation speed of cross flow fan, angle of attack, and incoming flow. The numerical analysis results of slotting on the leading edge show that the lift and thrust of the Fan Wing can be improved, but also the strength and position of the low-pressure vortices can be controlled. The results of flight tests show that the distributed lift and thrust of the Fan Wing can be directly applied to aircraft without the need for additional propulsion devices. In summary, the aerodynamic characteristics of the Fan Wing can be applied to electric short takeoff and landing (E-STOL) scenarios in urban air traffic.

**Keywords:** E-STOL; UAM; UAV; Fan Wing; aerodynamic characteristics; wind tunnel test



**Citation:** Du, S.; Zha, Y.; Zhao, Q. Research on Aerodynamic Test Validation and the Vector Force Control Method for an E-STOL Fan Wing Unmanned Aerial Vehicle. *Aerospace* **2024**, *11*, 55. <https://doi.org/10.3390/aerospace11010055>

Academic Editor: Hossein Zare-Behtash

Received: 18 October 2023  
Revised: 29 November 2023  
Accepted: 5 December 2023  
Published: 6 January 2024



**Copyright:** © 2024 by the authors. Licensee MDPI, Basel, Switzerland. This article is an open access article distributed under the terms and conditions of the Creative Commons Attribution (CC BY) license (<https://creativecommons.org/licenses/by/4.0/>).

## 1. Introduction

The concept of a Fan Wing [1,2] with distributed propulsion is a highly efficient and stable aircraft wing design that enables high lift capabilities. Each wing is equipped with a cross-flow fan located at the leading edge, which is powered by the engine and has an infinitely variable speed (shown in Figure 1a). This fan draws air from the front and propels it over the trailing edge of the wing, resulting in the simultaneous generation of lift and thrust (shown in Figure 1b). From the figure, it can be seen that the aerodynamic generation principle behind the Fan Wing is significantly different from that behind the Cycloidal propeller [3]. Both can form vector forces, and the latter has a more complex structure compared to the former. With the development of Urban Air Mobility (UAM), electric vertical or short takeoff and landing aircraft are attracting more and more attention; among which, aircraft with tilt function are the future development direction in terms of high-speed and economic performance [4–6]. The unique vector force formation mechanism (control the direction of vector force to achieve an effect similar to the tilting process of a tilting rotor), ultra short takeoff and landing characteristics, and simple structure of Fan Wing aircraft mean it has great application prospects in future air traffic travel.

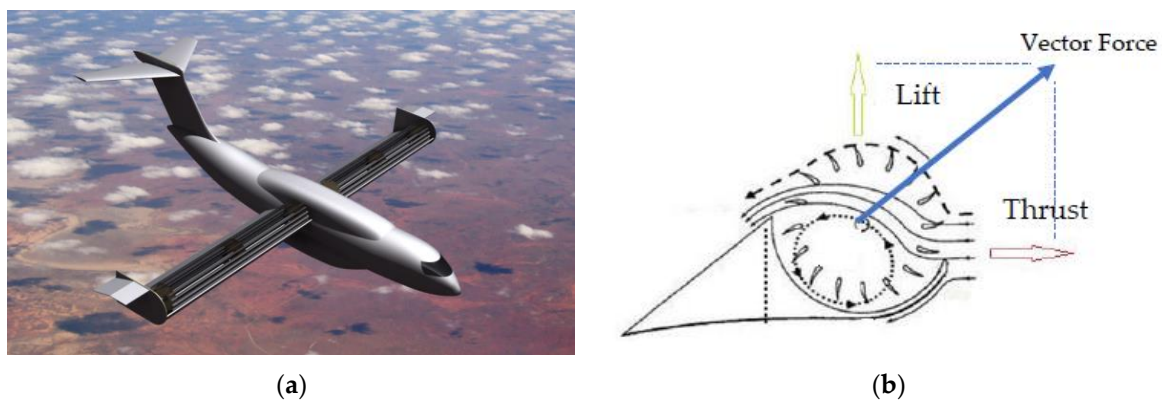


**Figure 1.** Introduction to the Fan Wing Principle: (a) Fan Wing aircraft; (b) Schematic diagram of the generation principle of lift and thrust on airfoil sections.

The innovative Fan Wing design also offers several advantages over conventional aircraft (Figure 2), including short take-off and landing (STOL) capabilities at low forward speeds, stall-free operation, and high power load. Recent research has focused on integrating Fan Wing technology into airfoils, demonstrating the potential for high lift performance through prototyping. Various experimental programs, such as the works of Kogler [7], Peebles [8], Seyfang [9,10], Foreshaw [11], Bayindir [12], Askari [13–16], Duddempudi [17], Dang [18,19], and Tang’s research team from Nanjing University of Aeronautics and Astronautics [20–22], have conducted detailed analysis of the aerodynamic characteristics of the Fan Wing through experimental and numerical simulations. These studies confirm that the geometric design parameters of the Fan Wing’s airfoil and cross-flow fan blade significantly influence the lift coefficient, thrust coefficient, and power load characteristics.



**Figure 2.** Application concept of Fan Wing aircraft ([www.fanwing.com](http://www.fanwing.com) (accessed on 1 October 2023)).

In recent years, numerical and experimental studies on Fan Wing blades have mainly been based on flat airfoil models, with little consideration of airfoil design. As most of the airfoil design work is based on numerical simulations, it is necessary to verify the accuracy of the computational results through wind tunnel tests to provide a basis for the aerodynamic layout design of the Fan Wing UAV. The relevant numerical simulation results indicate that the lift generated by the low-pressure vortex of the Fan Wing accounts for

more than 70% of the total lift. Therefore, it is necessary to observe and verify the formation process of the low-pressure vortex to study the variations in its intensity and position, and explore experimental verification platforms for decoupling control of Fan Wing force. That is, to control the direction of the vector force on the wing, similar to the tilting process of a tiltrotor.

In summary, this article will explore the theoretical and practical application directions of the Fan Wing based on wind tunnel tests, Fan Wing UAV design and flight tests, and numerical simulations of Fan Wing vector force control. In Section 2, wind tunnel tests on the Fan Wing model will be conducted using appropriate measurement techniques and methods to measure its lift, thrust, power, and flow field. In Section 3, we explore the theoretical and practical application directions of the Fan Wing by installing a slot on the front edge of the Fan Wing, and using numerical simulation analysis to control the vector force of the Fan Wing. In Section 4, a Fan Wing UAV will be designed and manufactured, and flight tests will be conducted to verify the integrated technologies of the Fan Wing structure, power drive, and flight control. In Section 5, a summary and outlook were provided for the entire article, and the research significance of this article was elaborated.

## 2. Fan Wing Aerodynamic Characteristics Test

### 2.1. Construction of the Test Model

The three-dimensional model of the Fan Wing used in this study is shown in Figure 3. The manufacturing process of the Fan Wing test section is depicted in Figure 4. The outer layer of the fixed wing of the Fan Wing is made of fiberglass material, while the inner layer is made of honeycomb panel material, providing structural support for the airfoil shape. The manufacturing process involves hot pressing using molds. The Fan Wing cross-flow fan is composed of 16 strips of carbon fiber blades with a droplet-shaped cross-section and left and right carbon fiber end plates, bonded together with high-strength adhesive. The blades are molded using molds, and the end plates were processed using a CNC carving machine. The Fan Wing test section has a straight wing configuration with no sweep angle or dihedral angle, and the airfoil profile was consistent along the wing-span direction. The dimensions of the Fan Wing test section profile are defined in Figure 5a, and the parameters of the Fan Wing blades are defined in Figure 5b. The specific parameter values are listed in Table 1.

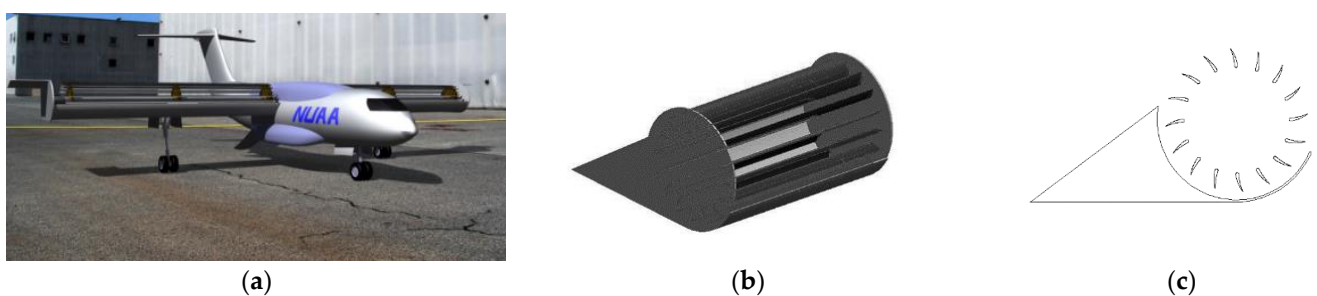


**Figure 3.** Three-dimensional model of the Fan Wing: (a) UAV model with Fan Wing; (b) Fan Wing test section model; (c) test section profile.

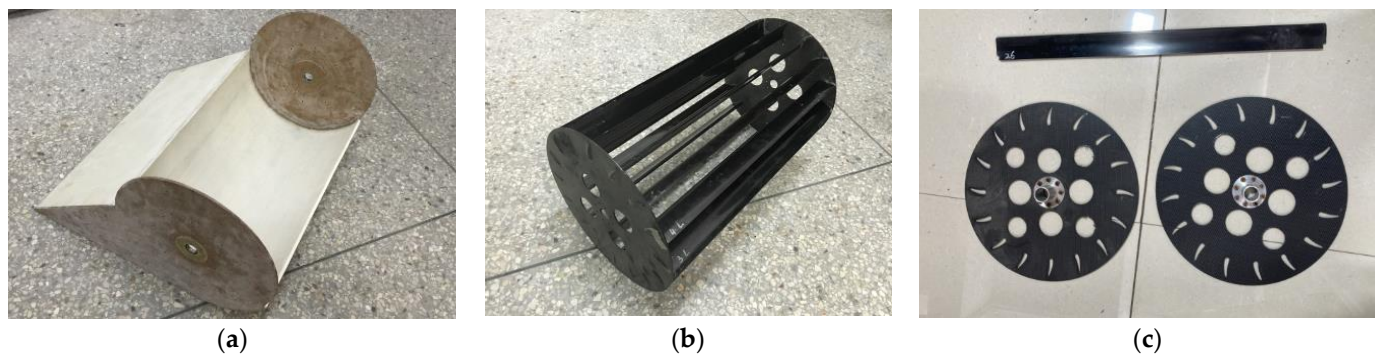


**Figure 4.** Manufacturing process of the Fan Wing test section: (a) fixed wing; (b) cross-flow fan; (c) blades and end plates.

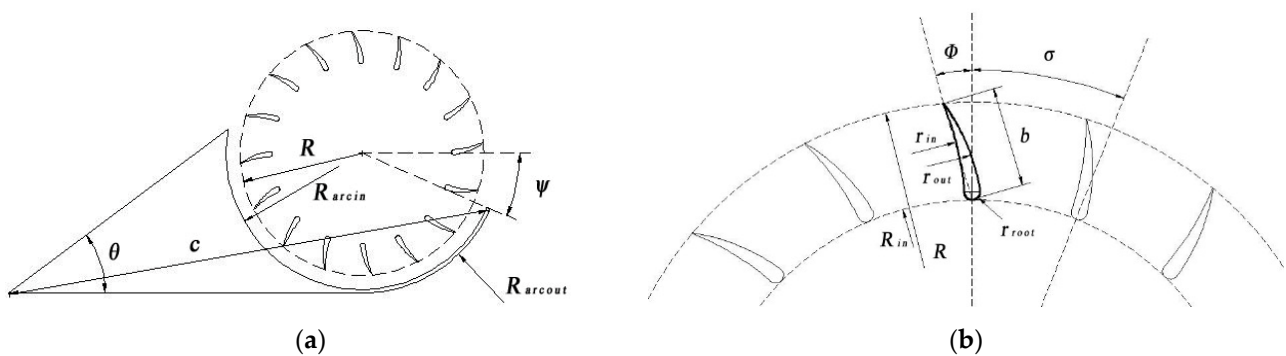


**Figure 5.** Definition of Fan Wing test section profile dimensions: (a) section size definition; (b) blade parameter definition.

**Table 1.** Parameters of the Fan Wing test section and blades.

Symbol	Part	Data
$N$	number of blades	16
$L_{span}$	span	0.5 m
$R$	cross flow fan radius	0.15 m
$R_{arcin}$	Inner diameter of circular groove	0.155 m
$R_{arcout}$	Outer diameter of circular groove	0.16 m
$c$	Chord	0.561 m
$\theta$	Angle between rear inclined planes	$18^\circ$
$\psi$	Leading edge opening angle	$24^\circ$
$b$	Blade width	0.036 m
$R_{in}$	Cross flow fan inner diameter	0.098 m
$r_{out}$	Blade outer arc radius	0.096 m
$r_{in}$	Blade inner arc radius	0.068 m
$r_{root}$	Blade reference arc radius	0.003 m
$\phi$	Blade tangential angle	$36.5^\circ$
$\sigma$	Blade installation angle	$22.5^\circ$

## 2.2. Establishment of Test Environment

The test setup is established in the wind tunnel at the National Key Laboratory of Helicopter Dynamics at Nanjing University of Aeronautics and Astronautics (Figure 6a), with the main parameters and resistance listed in Table 2. The rotor in the fan blade test section is connected to a brushless DC motor via a coupling, and the rotation speed of the fan blade rotor is adjusted by controlling the motor's speed (Figure 6b). The adjustment of the fan blade test section's angle of attack can be carried out through the angle of attack adjustment holes on the side panels of the test rig. Figure 6c shows the fan blade test section installed on the force measurement rig in the wind tunnel test section. The main body of

the force measurement rig is constructed with 4040 aluminum profiles. Four force sensors are vertically mounted on the upper part of the measurement rig to measure the lift of the fan blade model test section (Figure 6d), and one force sensor is horizontally installed in the middle of the measurement rig to measure the thrust of the fan blade model test section (Figure 6e). Main parameters of measurement and control equipment listed in Table 3.

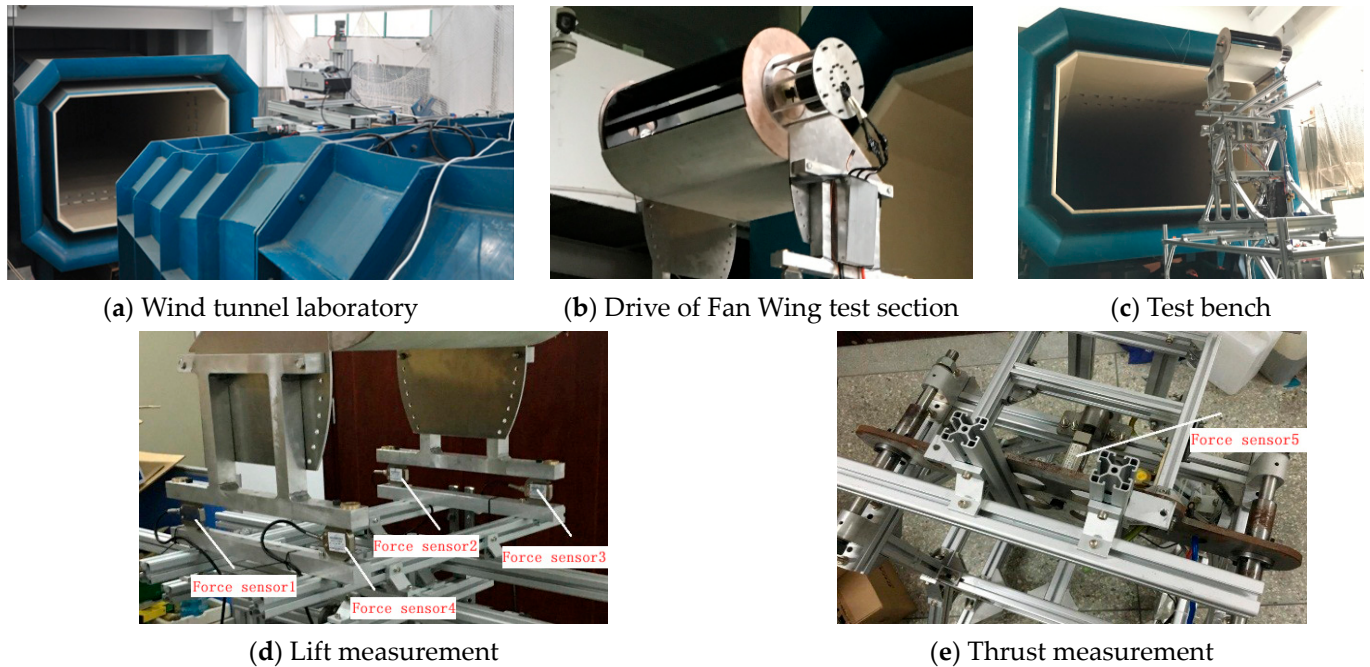


**Figure 6.** Construction of Fan Wing test environment.

**Table 2.** Main parameters of wind tunnel.

Part	Data
Wind tunnel caliber (height × width)	2.4 m × 3.4 m
Stable wind speed range	5~50 m/s
Average airflow deviation angle	$\Delta\alpha \leq \pm 0.1^\circ$ $\Delta\beta \leq \pm 0.1^\circ$
Turbulence	$\varepsilon \leq 0.1\sim 0.14\%$
Velocity Field Coefficient	$\Delta\mu \leq 0.5\%$

**Table 3.** Main parameters of measurement and control equipment.

Part	Brand/Specification	Quantity	Parameter
Force sensor	−100~+100 kg	5	accuracy $\pm 0.03\%$
Speed Sensor	0~9999 r/min	1	accuracy $\pm 0.1\%$
Data Acquisition Software	Anhui Dayang, China	1	5 channels
Wireless data transmission module	Loar	2	RS232
DC power	Agilent N8900	1	accuracy $\pm 0.1\%$
Brushless DC motor	HACKER	1	50 V 10 KW
Electronic speed control	HACKER	1	50 V 220 A
Particle Image Velocimetry	LaVison PIV	1	accuracy RMS < 0.04

The test setup employs a high-speed wireless data acquisition module to collect data from the force sensors in the fan blade test section. The collected data are then filtered, displayed, and recorded using a five-channel data acquisition software. The measurement and control principles are illustrated in Figure 7a, and the collection and monitoring equipment can be seen in Figure 7b.

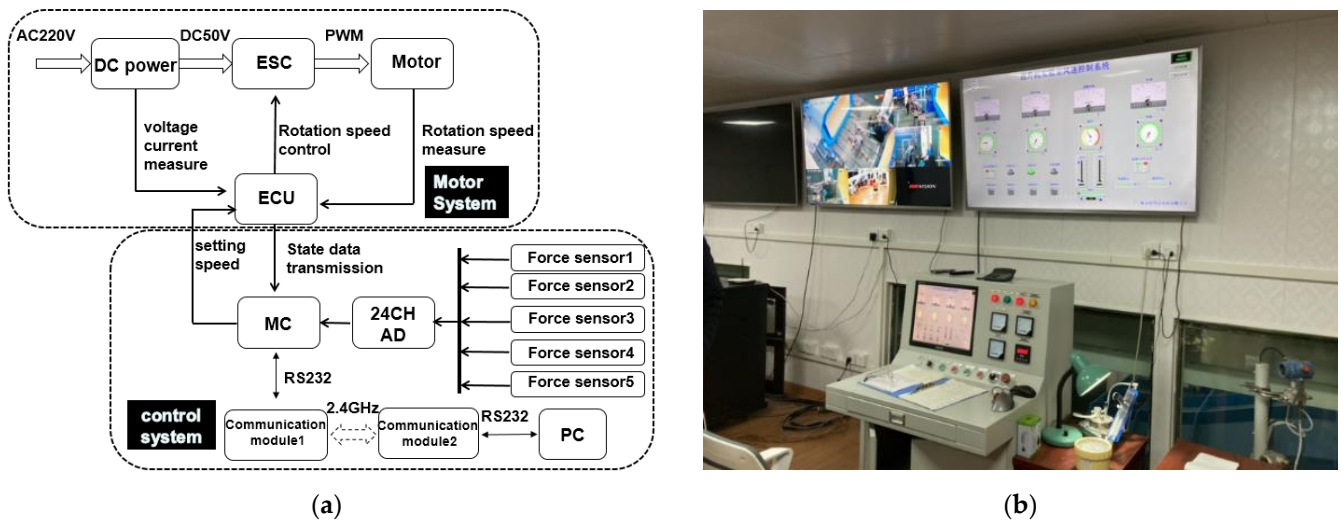


**Figure 7.** Construction of experimental measurement and control data acquisition system: (a) measurement and control system architecture; (b) measurement and control instruments and equipment.

2.3. Test Scheme

The tests are divided into three main parts:

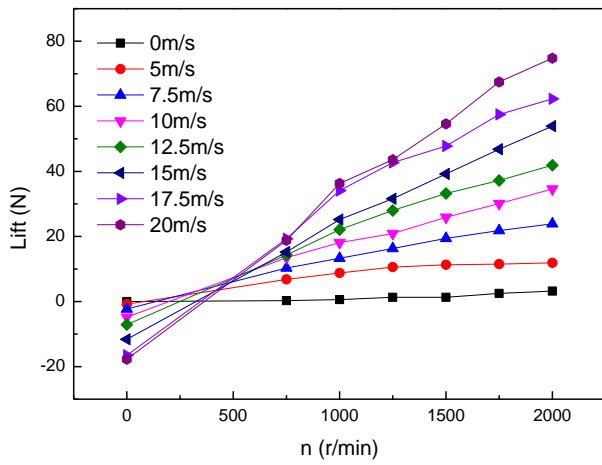
- a. The first part involves measuring the propulsive force of the fan blade, which includes measuring both the lift and thrust of the fan blade. The measurement conditions are outlined in Table 4.
- b. The second part focuses on measuring the flow direction and velocity of the airflow accelerated by the fan blade rotor.
- c. The third part involves the observation and verification of the formation process of the low-pressure vortex inside the fan blade.

**Table 4.** Fan Wing test section test status table.

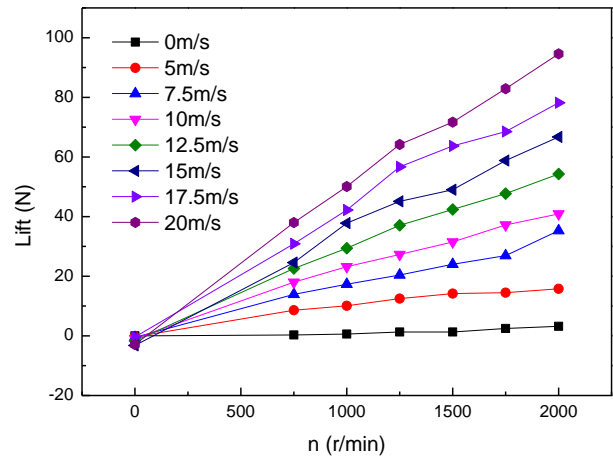
Parameters	Data
Rotation speed (r/min)	750, 1000, 1250, 1500, 1750, 2000
Incoming flow velocity (m/s)	0, 5, 7.5, 10, 12.5, 15, 17.5, 20
Angle of attack (°)	-10, -5, 0, +5, +10, +15, +20, +25, +30

2.4. Test Results and Analysis

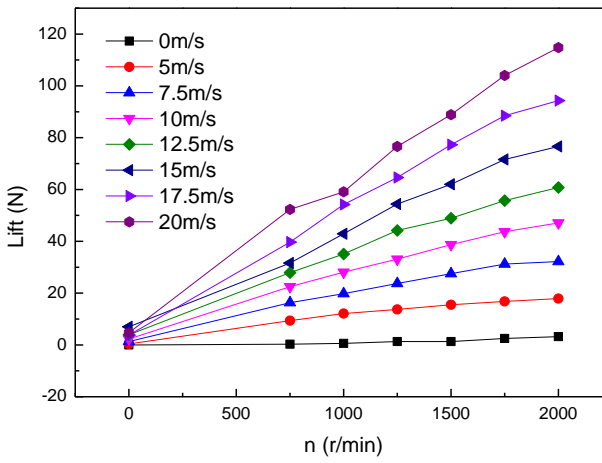
Figure 8 presents the experimental results for the fan blade lift as a function of the angle of attack, incoming flow velocity, and rotor speed. From the graph, it can be observed that, with a constant incoming flow velocity and angle of attack, the fan blade lift increases as the rotor speed increases. Similarly, with a constant rotor speed and angle of attack (greater than 750 r/min), the fan blade lift increases with an increase in the incoming flow velocity. Additionally, with a constant incoming flow velocity and rotor speed, the fan blade lift increases with an increase in the angle of attack. The magnitude of the fan blade lift is positively correlated with the angle of attack, incoming flow velocity, and rotor speed. Analyzing the growth rate trends of the fan blade lift curve in Figure 8, it can be observed that, at lower angles of attack (<15°), a higher incoming flow velocity leads to a greater rate of increase in the fan blade lift. However, at higher angles of attack (>15°), the rate of increase in the fan blade lift tends to decrease. From Figure 8a,b, it can be seen that the fan blade can still generate lift even at negative angles of attack. Furthermore, as the angle of attack changes from -10° to +30°, the fan blade lift continues to increase. This confirms the wide range of applicable angle of attacks for the fan blade and its ability to operate at high angles of attack without stalling.



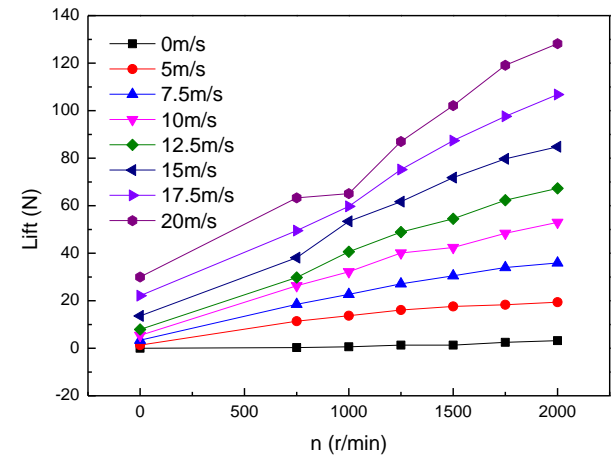
(a)  $\alpha = -10^\circ$



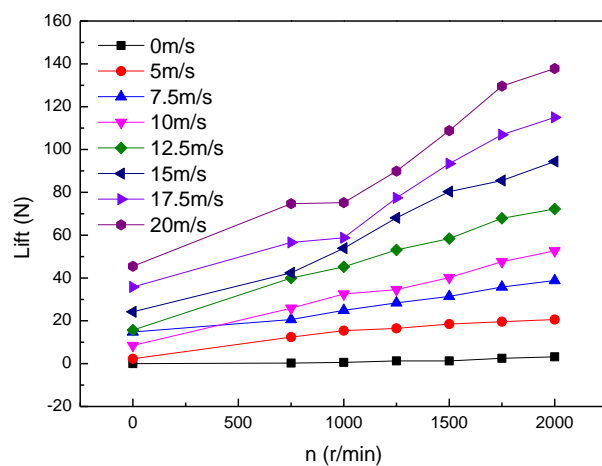
(b)  $\alpha = -5^\circ$



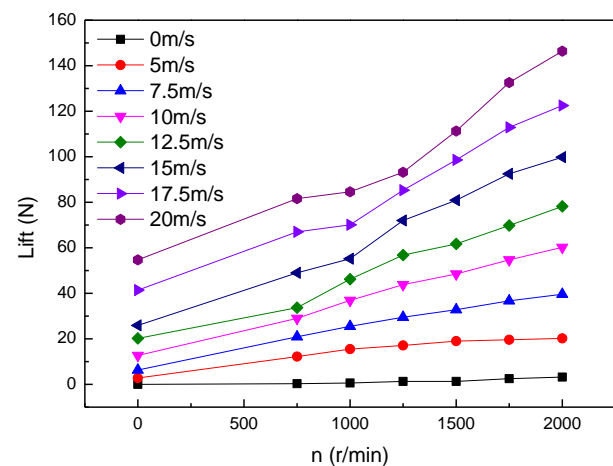
(c)  $\alpha = 0^\circ$



(d)  $\alpha = 5^\circ$

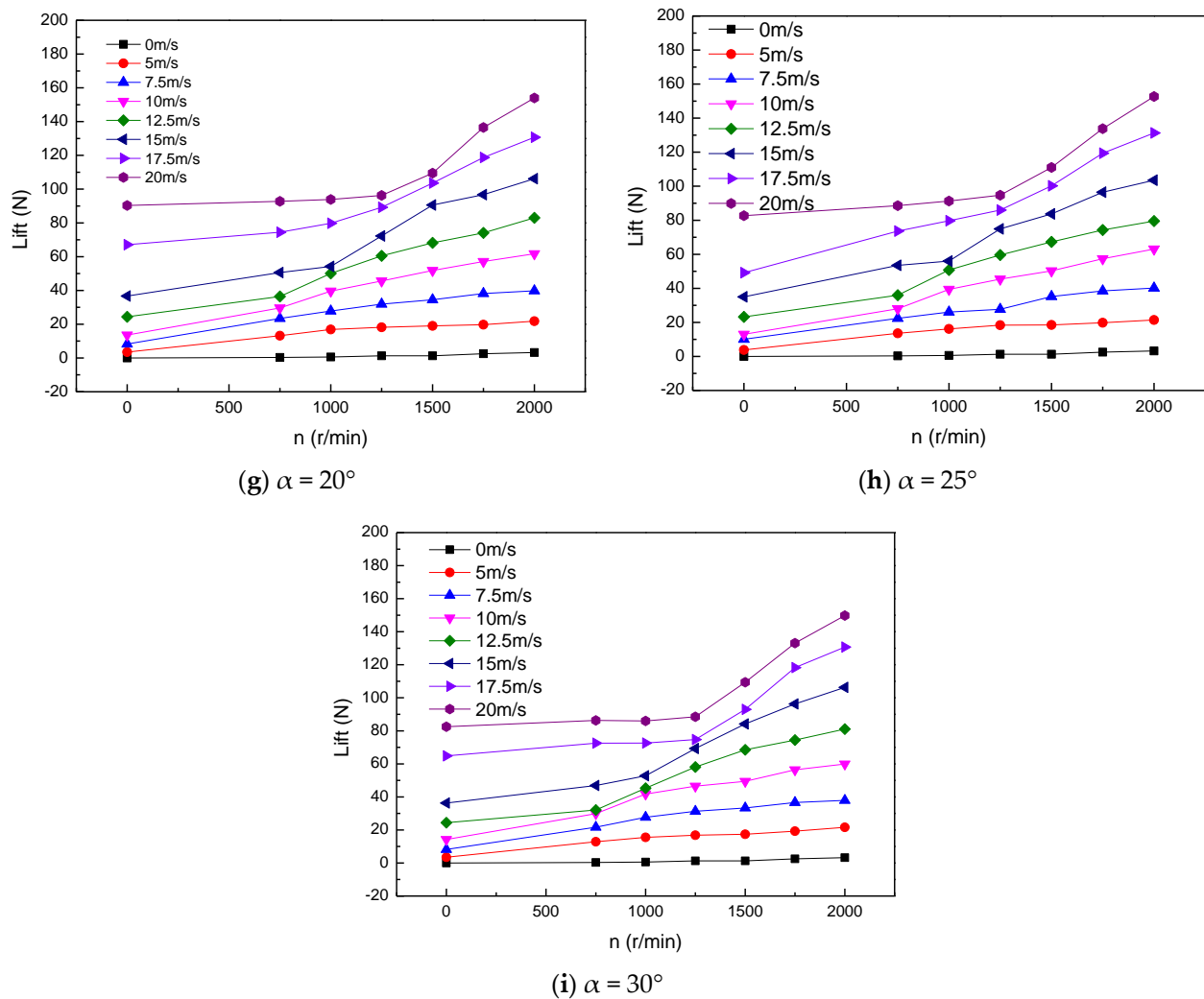


(e)  $\alpha = 10^\circ$



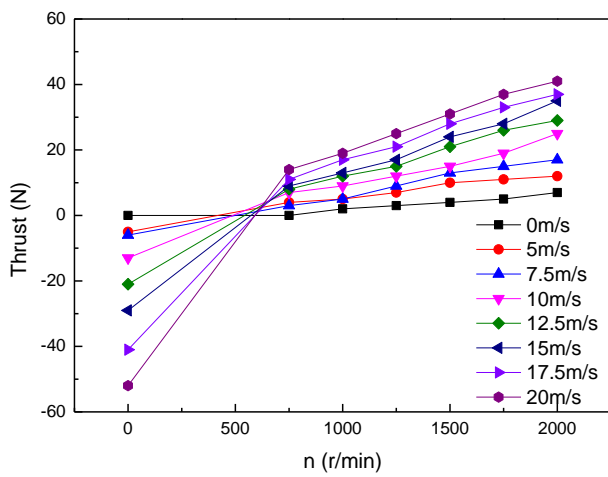
(f)  $\alpha = 15^\circ$

Figure 8. Cont.

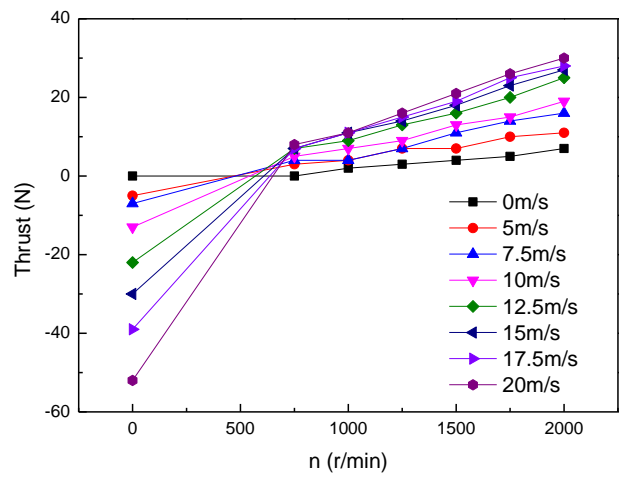


**Figure 8.** Variation curves for Fan Wing lift with rotation speed of cross flow fan, inflow velocity, and angle of attack.

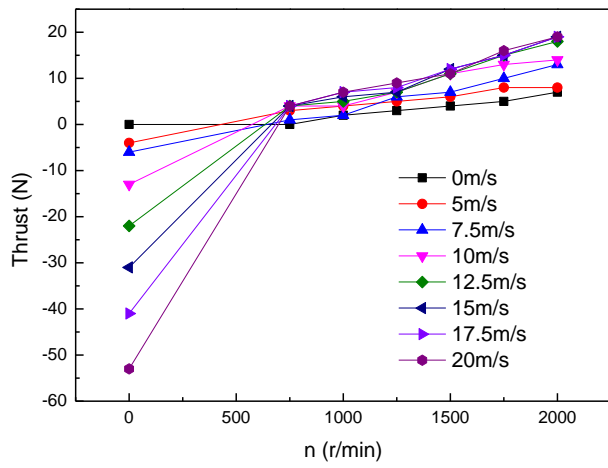
Figure 9 displays the experimental results for fan blade thrust as a function of the angle of attack, incoming flow velocity, and rotor speed. From the graph, it can be observed that, within the range of  $-10^\circ$  to  $+5^\circ$  of the angle of attack, with a constant incoming flow velocity and angle of attack, the fan blade thrust increases with an increase in the rotor speed. Similarly, with a constant rotor speed and angle of attack (greater than  $750$  r/min), the fan blade thrust increases with an increase in the incoming flow velocity. Additionally, with a constant incoming flow velocity and rotor speed, the fan blade thrust decreases and the growth rate becomes relatively smaller as the angle of attack increases. As the angle of attack continues to increase, the thrust direction of the fan blade changes, leading to the generation of drag. The greater the angle of attack, the larger the drag. Comparing the maximum thrust of  $41$  N at an angle of attack of  $-10^\circ$  with the maximum drag of  $26$  N at an angle of attack of  $+30^\circ$ , the rate of change is approximately 2.6 times, indicating that the angle of attack is the key factor influencing the fan blade thrust. From the graph, it can also be analyzed that by adjusting the angle of attack without changing the flight heading, the fan blade aircraft can be controlled to fly forwards or backwards, and even hover in the air. This aligns with the vertical takeoff and short takeoff and landing characteristics of the fan blade aircraft. The graph also shows that when the rotor speed is  $0$  r/min, a higher incoming flow velocity results in a higher drag of the fan blade. This is related to the large projected area of the fan blade's thick airfoil in the direction of the incoming flow, and it further demonstrates the application of the fan blade in low-speed flight scenarios.



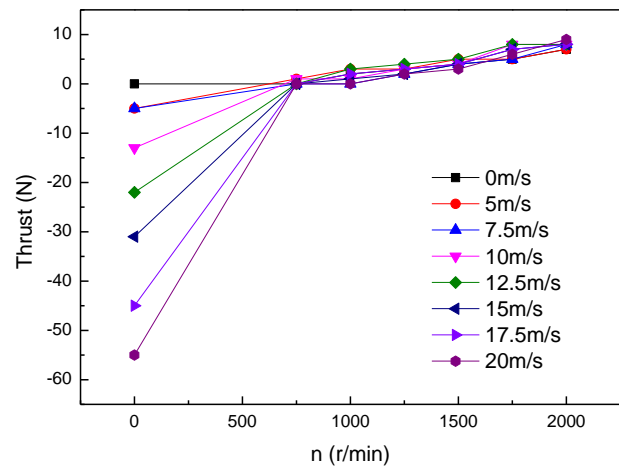
(a)  $\alpha = -10^\circ$



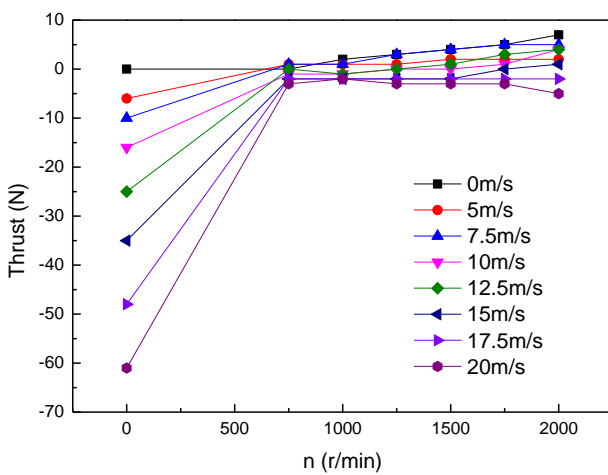
(b)  $\alpha = -5^\circ$



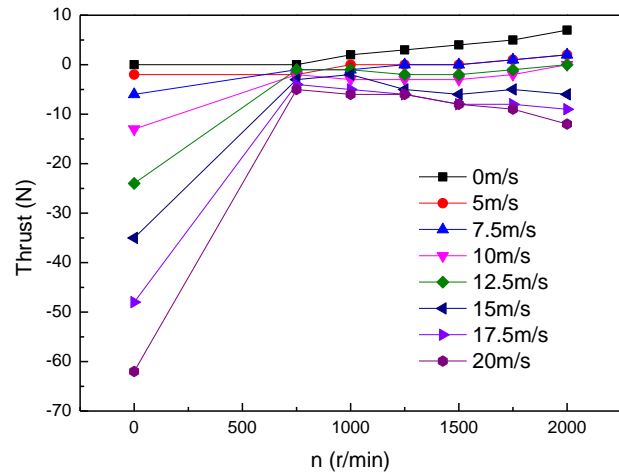
(c)  $\alpha = 0^\circ$



(d)  $\alpha = 5^\circ$



(e)  $\alpha = 10^\circ$



(f)  $\alpha = 15^\circ$

Figure 9. Cont.

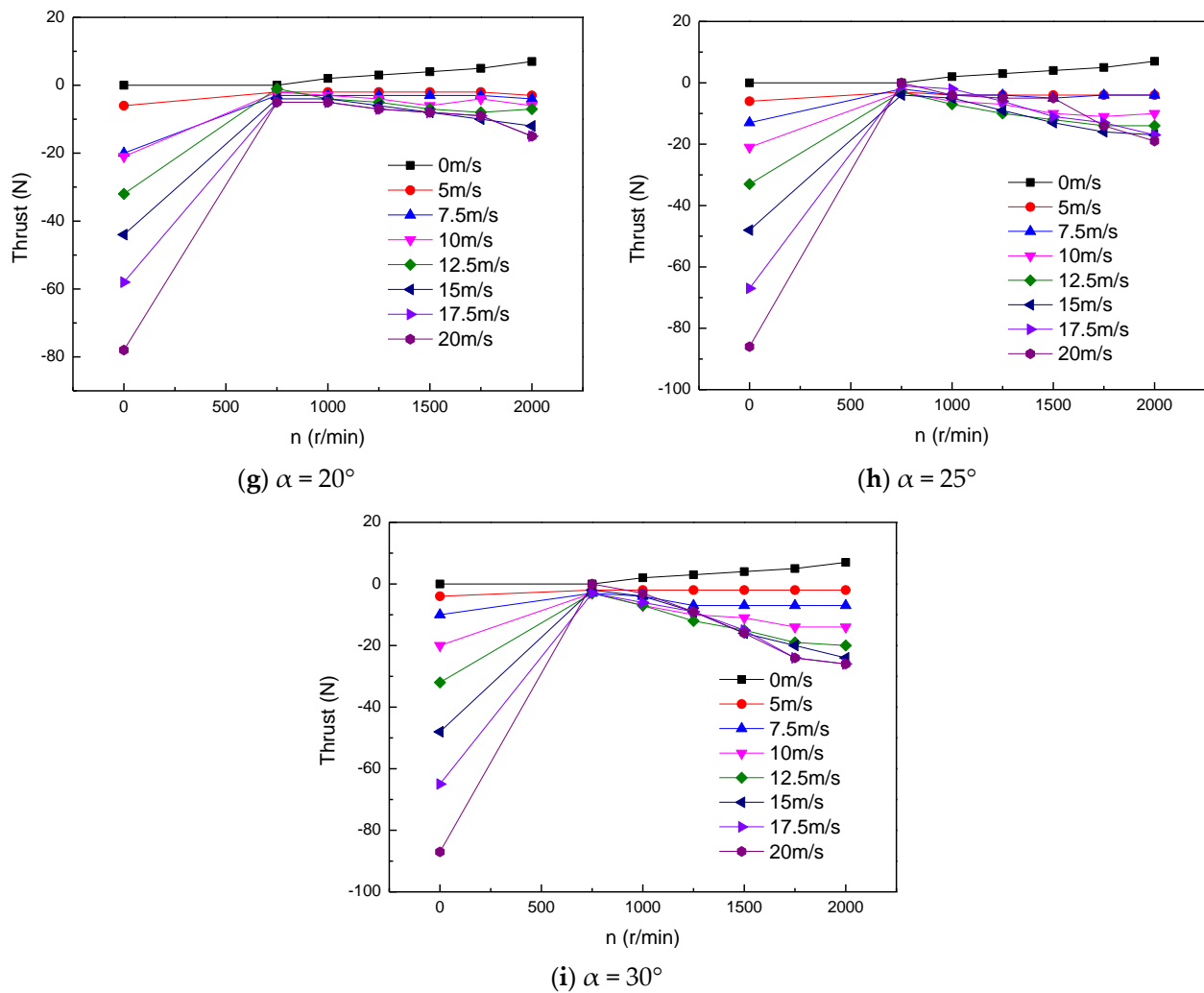
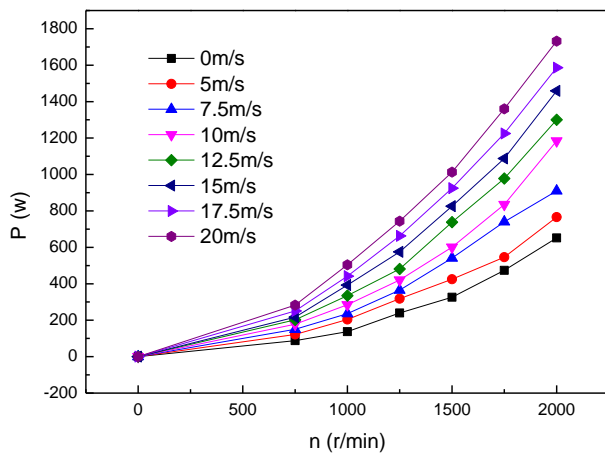


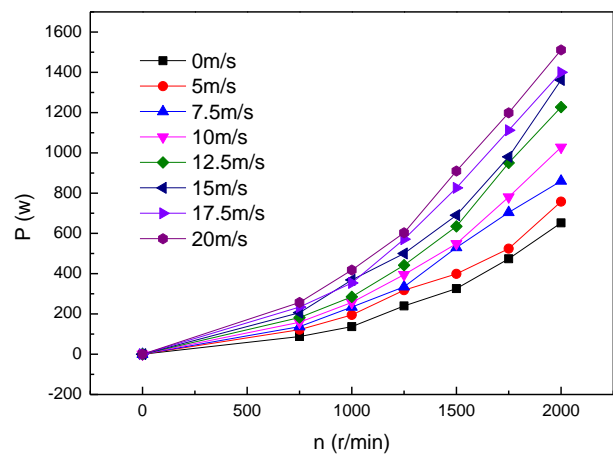
**Figure 9.** Variation curves for Fan Wing thrust with rotation speed of cross flow fan, inflow velocity, and angle of attack.

In the test, the curve results in Figure 10 showcased the variation in fan blade power with respect to the angle of attack, inflow velocity, and the rotation speed of the cross-flow fan. It can be observed from the graph that, when inflow velocity and angle of attack remain constant, the fan blade power increases with the increase in rotor speed. Similarly, when inflow velocity and rotor speed remain constant, the fan blade power decreases with the increase in angle of attack. During the variation process of angle of attack from  $-10^\circ$  to  $+10^\circ$  (with rotation speed of cross flow fan and angle of attack unchanged and greater than 750 r/min), the fan blade power increases with the increase in inflow velocity. However, during the variation process of angle of attack from  $+15^\circ$  to  $+30^\circ$ , the fan blade power decreases with the increase in inflow velocity.

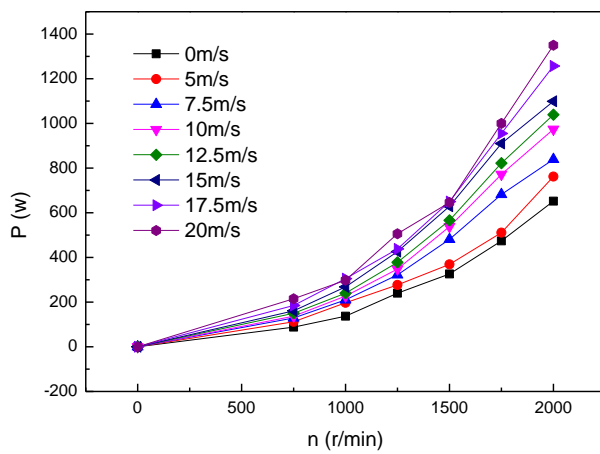
Based on the experimental results, the lift-to-thrust ratio curve for a fan blade with an angle of attack of  $5^\circ$  was calculated (Figure 11). From the graph, it can be observed that the maximum lift-to-thrust ratio occurs at a fan blade rotor speed of 1000 r/min and an inflow velocity of 20 m/s, reaching 65. This value is significantly higher than conventional wings, indicating the fan blade aircraft's capability for high load flights at low speeds.



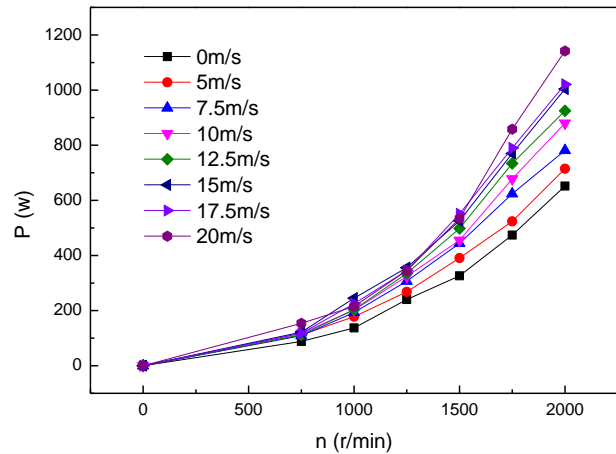
(a)  $\alpha = -10^\circ$



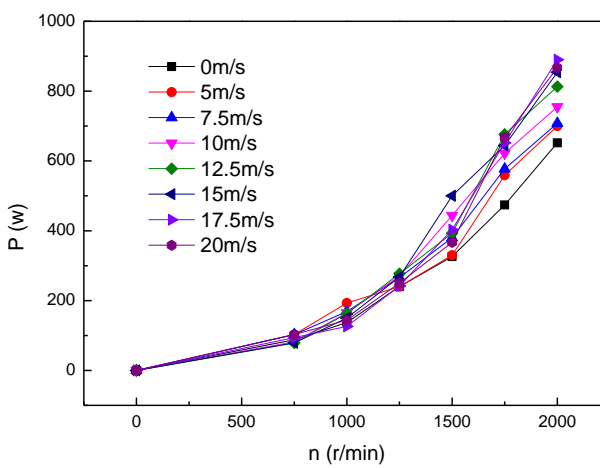
(b)  $\alpha = -5^\circ$



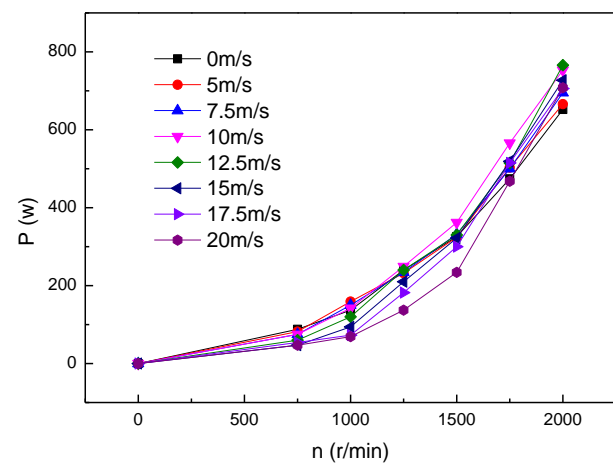
(c)  $\alpha = 0^\circ$



(d)  $\alpha = 5^\circ$



(e)  $\alpha = 10^\circ$



(f)  $\alpha = 15^\circ$

Figure 10. Cont.

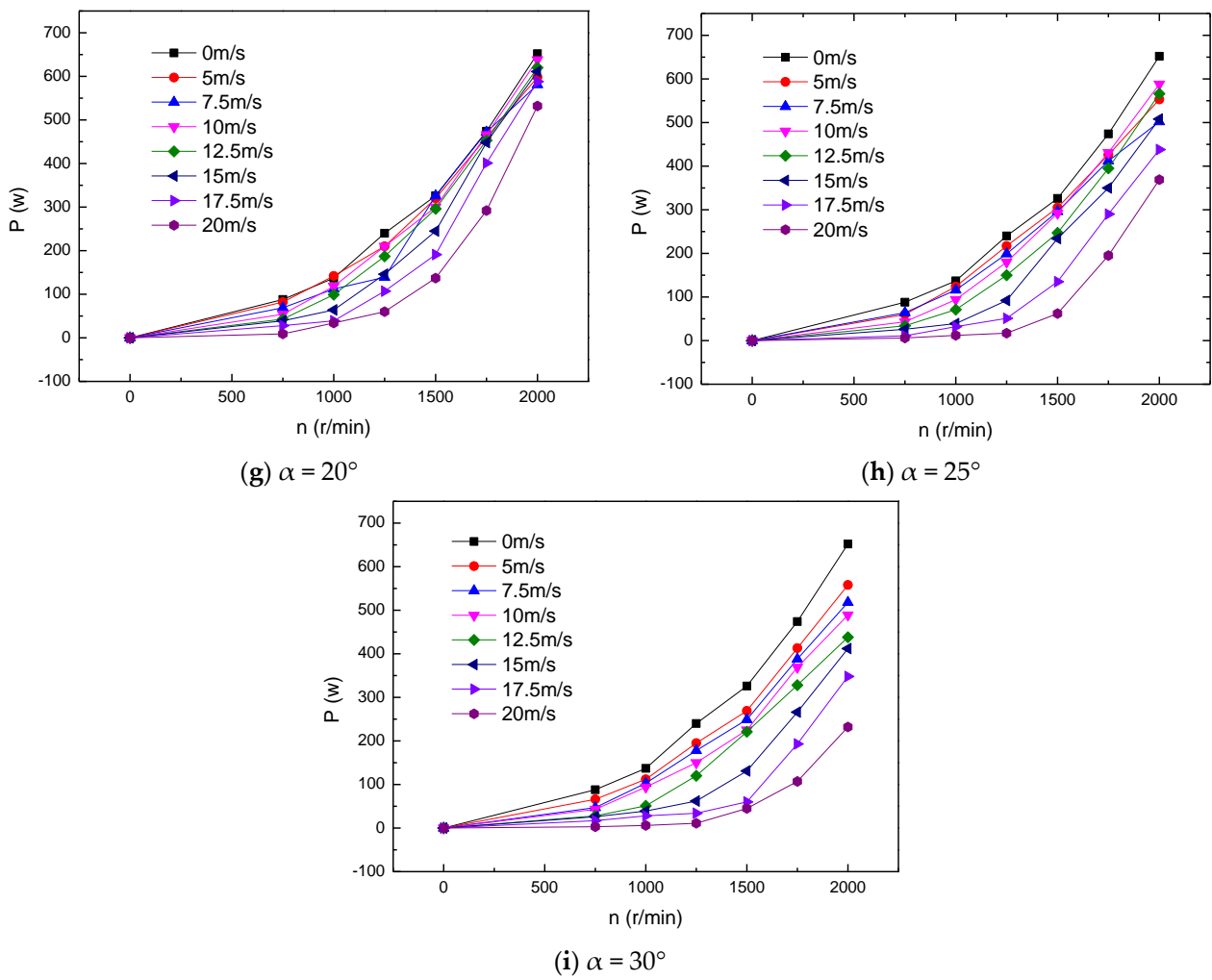


**Figure 10.** Variation curves for Fan Wing power with rotation speed of cross flow fan, inflow velocity, and angle of attack.

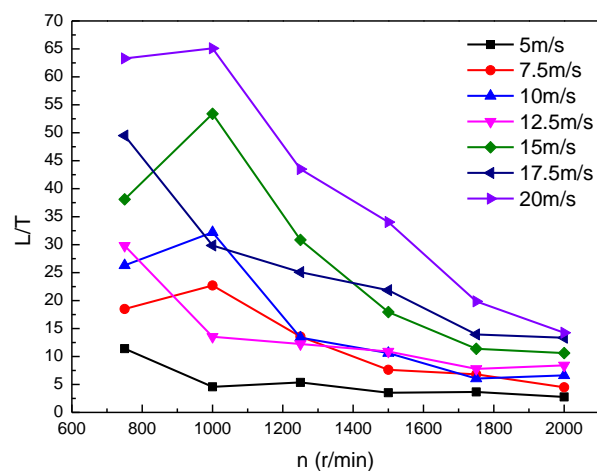


**Figure 11.** Curve of Fan Wing lift to thrust ratio variation.

Further analyzing the aerodynamic efficiency of the fan blade, the power load at a rotor speed of 1500 rpm and an inflow velocity of 10 m/s was calculated. From Figure 12a, it can be observed that the larger the angle of attack of the fan blade, the higher the power load, with the maximum power load being approximately 23 g/W. Analyzing the proportion of

lift and thrust in relation to the propulsive force (Figure 12b), the proportion of lift remains relatively consistent with slight variations in the range of angle of attack, maintaining above 80% and reaching over 95% at positive angles of attack. On the other hand, the proportion of thrust experiences more noticeable variation with changes in the angle of attack, showing a tendency for thrust reduction. When the angle of attack exceeds 10°, it results in the generation of drag.

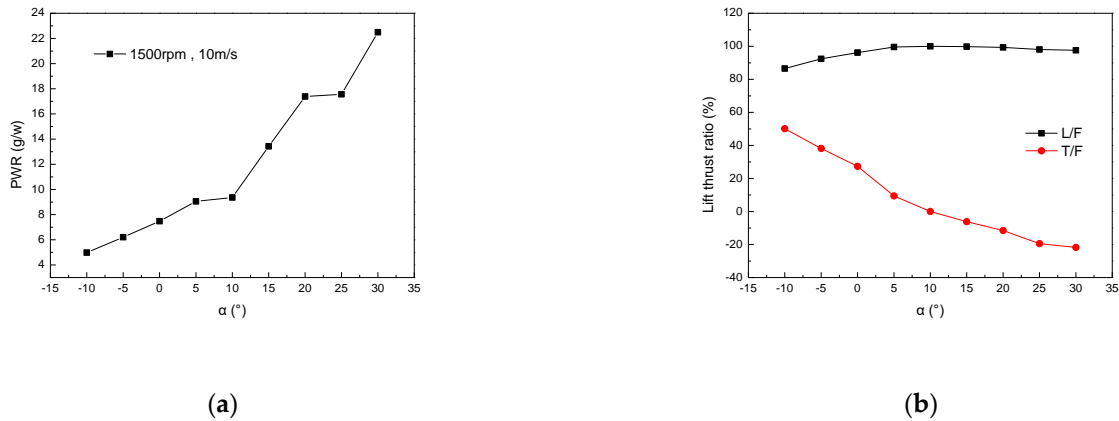


**Figure 12.** Curve of Fan Wing aerodynamic characteristics with angle of attack: (a) power load; (b) lift–thrust ratio.

Continuing with the analysis of the influence of rotor speed on power load of the fan blade (Figure 13a), it can be observed from the graph that higher rotor speeds result in lower power loads for the fan blade. The power load at the lowest rotor speed is more than four times that at the highest rotor speed, indicating a high aerodynamic efficiency at low speeds. Analyzing the proportion of lift and thrust in relation to the propulsive force with respect to changes in rotor speed (Figure 13b), the proportion of lift remains relatively constant, while the proportion of thrust increases with higher rotor speeds, transitioning from drag to thrust.

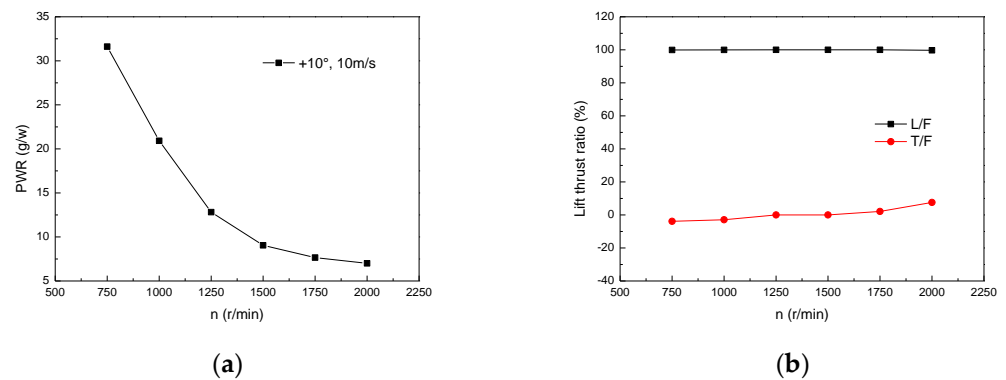


**Figure 13.** Curve of Fan Wing aerodynamic characteristics with rotation speed of cross flow fan: (a) power load; (b) lift–thrust ratio.

In Figure 14a, the influence of inflow velocity on power load is depicted. It can be observed from the graph that, as the inflow velocity increases, the power load also increases, indicating an enhancement in aerodynamic efficiency. Analyzing the proportion of lift and thrust in relation to the propulsive force with respect to changes in inflow velocity (Figure 14b), the proportion of lift remains relatively constant, while the proportion of thrust gradually decreases with higher inflow velocities, eventually reaching a stable state.

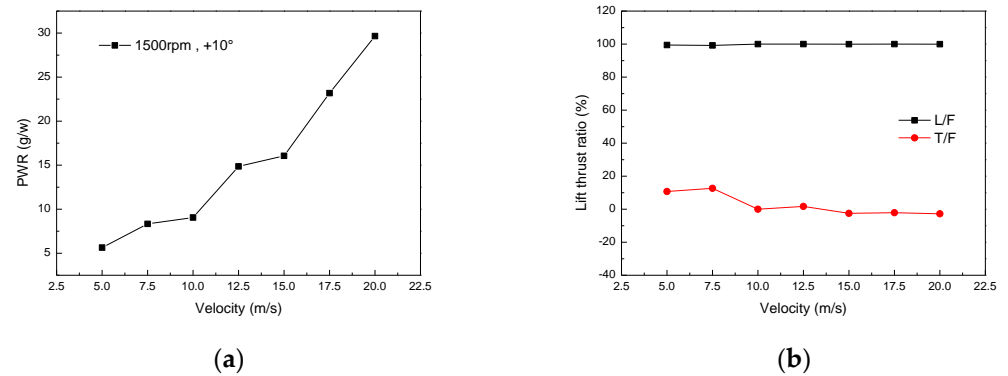


**Figure 14.** Curve of Fan Wing aerodynamic characteristics with inflow velocity: (a) power load; (b) lift–thrust ratio.

### 3. Fan Wing Vector Force Control Method

The leading edge opening angle is the biggest factor affecting the lift and thrust of the Fan Wing after the size of the wing airfoil and cross-flow fan was determined. Within a certain opening angle, the leading edge opening angle increases, the lift and thrust increase, and the thrust increases significantly. The simplest way to control the opening angle of the Fan Wing is to create slots on the leading edge winglet, which can change the opening size of the leading edge by moving the baffle of the servo to cover the slotted area, so as to improve the aerodynamic characteristics of the Fan Wing. In this section, the numerical simulation will be used to investigate the aerodynamic control effect of the leading edge slotted on the Fan Wing.

#### 3.1. Definition of Leading Edge Slotting

Based on the datum Geometric model, the slot positions are shown in Figure 15a. The slot position is defined by the angle between the slot centerline and the X-axis, as shown in Figure 15b,c, and the corresponding slot positions were placed at  $43^\circ$  and  $43\text{--}52^\circ$ . The definition of slot width is as follows: the centerline of the slot extends  $2^\circ$  on both sides, which means the slot width is within the range of  $4^\circ$ , and the length was approximately 10.88 mm. The double slot spacing is  $5^\circ$ .

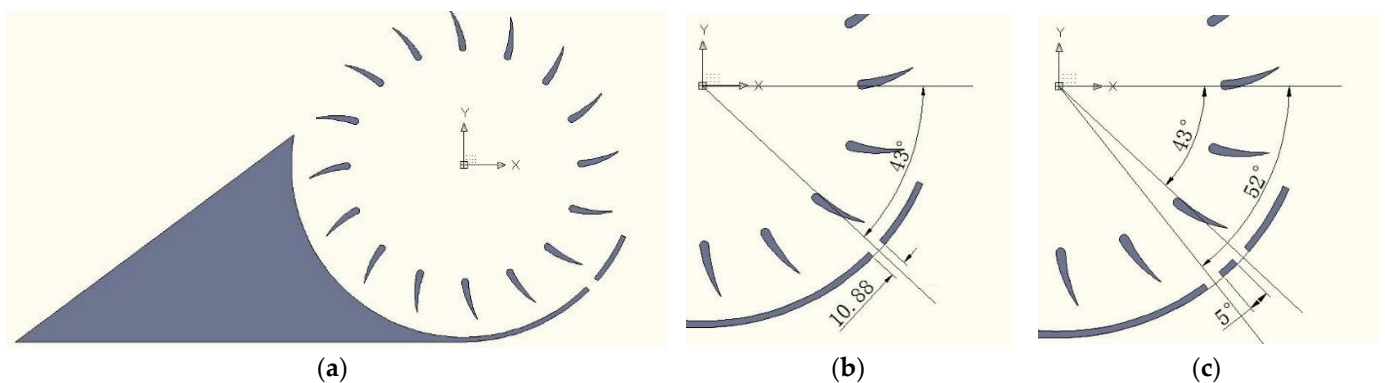


**Figure 15.** Definition of slot position: (a) aerofoil section; (b) single slot; (c) double slot.

#### 3.2. Numerical Calculation Method

The article uses the RANS (Reynolds-Averaged Navier–Stokes) equations as the governing equation, adopts the SIMPLE (Semi-Implicit Method for Pressure Linked Equations) algorithm based on staggered grids, selects the RNG (Reynolds-Averaged Navier–Stokes) k-epsilon model, slip grid model, and considers the influence of wall viscosity using standard wall functions to establish a numerical simulation method for the flow field of a Fan Wing. The flow field of a Fan Wing’s wing was complex. In order to better complete the

numerical simulation, the flow field is divided into different regions, and the grids of each region are generated separately. Structural grids are used for simple and periodic regions, while unstructured grids are used for complex regions. Then, the grids of each region were merged to generate a mixed grid for the overall flow field. The grid partitioning process is shown in Figure 16. The grid partitioning software uses ICEM. The numerical simulation software used is FLUENT2020R1. In two-dimensional numerical simulations, the flow field domain is generally chosen to be 10 to 20 times the chord length. Based on experience and computational attempts, this article selects a rectangular area as the computational domain, with the rotating center of the Fan Wing's cross-flow fan located 6 m from the inlet and 8 m from the outlet. The chord length of the Fan Wing in this article is 0.56 m, and the minimum boundary of the calculation area is about 15 times the characteristic length. During normal flight of a Fan Wing aircraft, this area is greatly affected, and the boundary of the computational domain will not cause aerodynamic interference to the wings. Therefore, studying the influence of the leading edge of the Fan-Wing's wing on aerodynamic performance is a reasonable choice. The length and width of the flow field are  $14 \times 8$  m, and the number of grid elements is about 450,000. Mesh-independency studies were also conducted with three successive meshes: coarse, medium, and fine meshes. The coarse mesh has 295,826 elements. The medium mesh has 449,558 elements. The fine mesh has 892,276 elements. The study has shown that differences in the results from the coarse and medium meshes are significant, while differences in the results between the medium and fine meshes are almost negligible. Hence, it was decided to use the medium mesh as the baseline for further simulation.

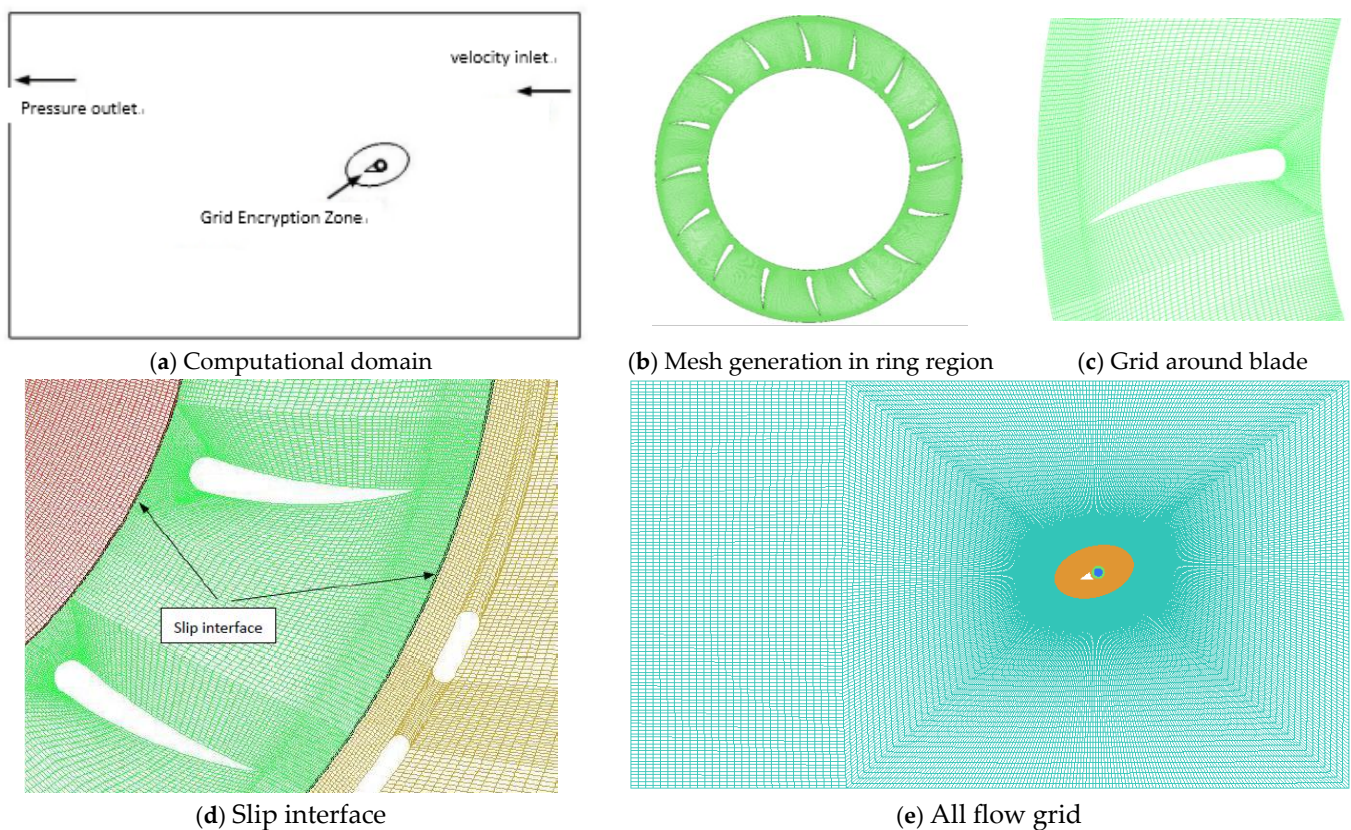


**Figure 16.** The process of meshing Fan Wing.

### 3.3. Examples Verification

In order to verify the accuracy of the numerical algorithm, the results were compared with those of the wind tunnel test. The dimensions of the experimental model and the numerical calculation model are consistent. In the experiment, the inflow velocity was set at 5 m/s, the angle of attack was  $0^\circ$ , and the rotational speed range of the cross-flow fan

was 400–1200 rpm. It can be seen that the numerical results for the Fan Wing are in good agreement with the experimental results (Figure 17). The maximum error is less than 10%, and the error of the cross-flow fan at high speed is less than 5%. Therefore, the general numerical simulation software and its numerical calculation method used in this article are reliable. The formulas for lift coefficient (CL) and thrust coefficient (CT) are defined as follows:

$$CL = \frac{L}{(1/2)\rho V^2 S} \quad CT = \frac{T}{(1/2)\rho V^2 S}$$

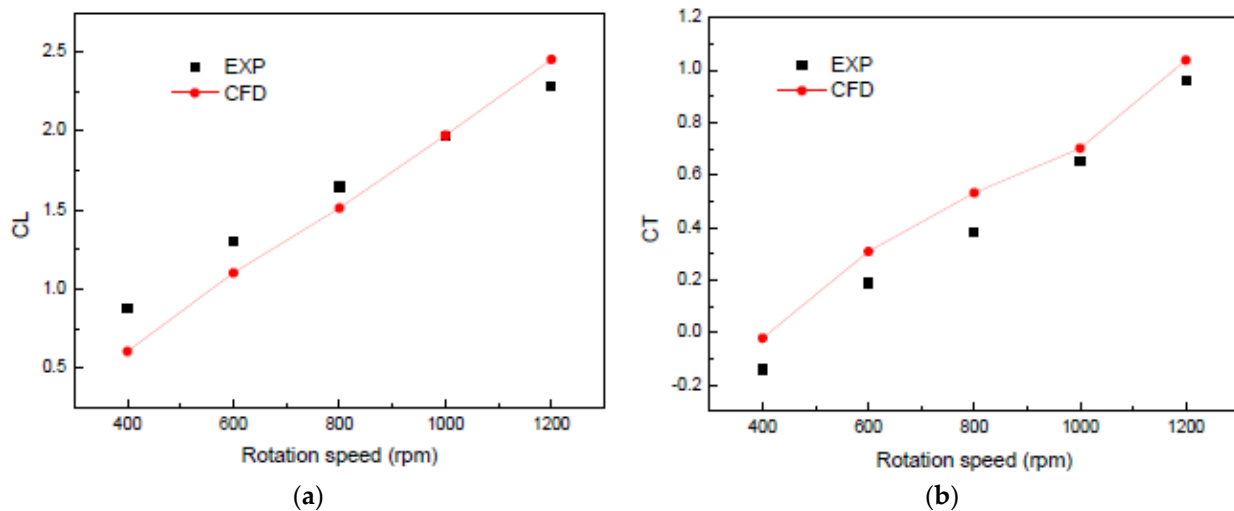


**Figure 17.** Comparisons between numerical calculation and experimental results: (a) lift coefficient; (b) thrust coefficient.

Reference area:

$$S = c \cdot L_{span}$$

$\rho$  for standard air density,  $V$  for incoming flow velocity.

### 3.4. Calculation Results and Analysis

#### 3.4.1. Effect of Slot Width on the Aerodynamic Performance of the Fan Wing

The calculation results under different inflow conditions, when the slot widths are  $1^\circ$ ,  $2^\circ$ ,  $3^\circ$ ,  $4^\circ$ ,  $5^\circ$ , and  $0^\circ$  (reference model without slot), and the slot position is  $43^\circ$ , are compared and analyzed. Comparing the calculation results of different slot widths in Figure 18, it can be seen that after slotting, the flow can enter the cross-flow fan through the slot, and as the slot width increases, more incoming flow enters the cross-flow fan. The flow velocity in the inclined section and leading edge arc section of the upper wing surface increases. As the slot width increases, the influence of the cross-flow fan's rotation on the flow field near the wing increases, and the change in direction of incoming flow entering the cross flow fan increases. At the same time, the trailing vortex pulled out by the leading edge of the wing separated by the slot gradually decreases with the increase in slot width.

In order to more clearly display the force changes of the Fan Wing before and after slotting, as shown in Figure 19, a comparative analysis was conducted on the surface static-pressure distribution on the Fan Wing segment. The comparison of the static-pressure distribution on the wing surface between the reference model and the slot width of  $1^\circ$  and  $5^\circ$  was obtained. As shown in the figure, after slotting, the pressure on the inner surface of the inclined section of the upper wing surface and the curved section of the leading edge of the wing decreases. The larger the slot width, the more the pressure decreases, and the static pressure on the lower surface of the wing remains basically unchanged. The pressure on the inner surface of the arc-shaped segment near the leading edge slot location rapidly increases, and as the slot width increases, the pressure increases. However, the leading

edge segment separated by the slot becomes shorter as the slot width increases, and the pressure difference between the inner and outer surfaces increases, causing the lift of the wing to increase with the slot width, but the increase is not significant.

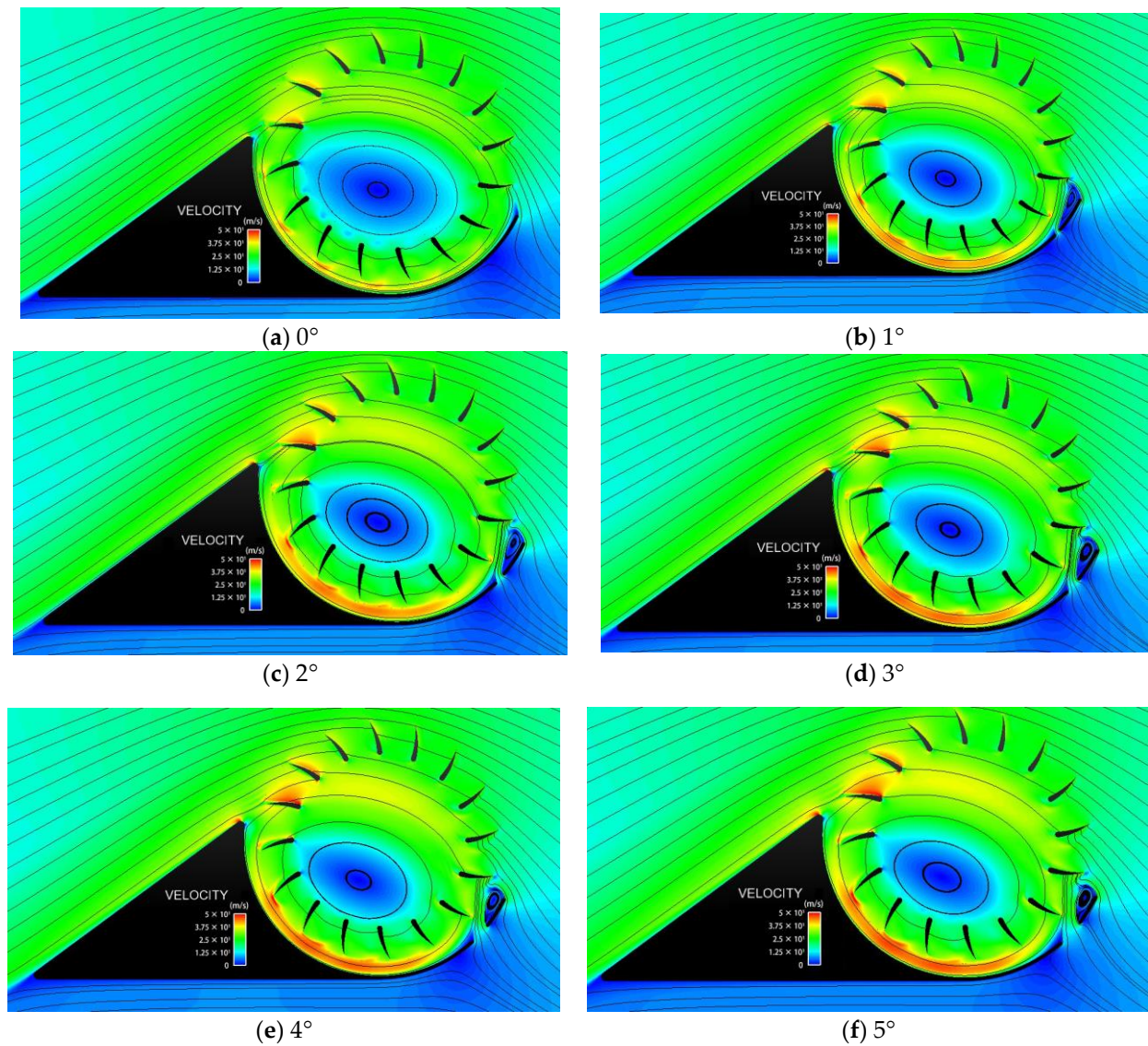


Figure 18. Cloud and streamline diagrams of different slot widths and velocities.

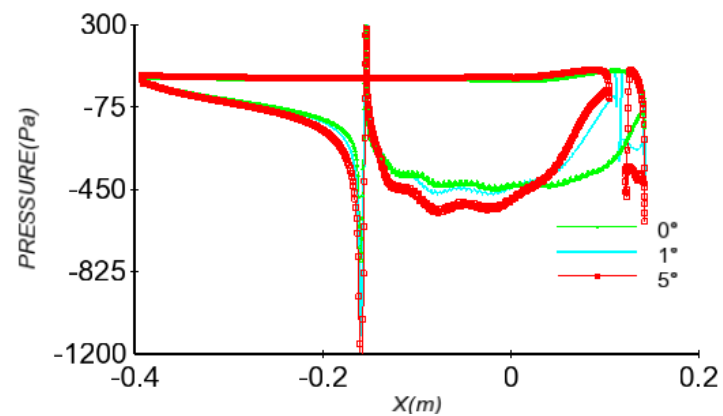
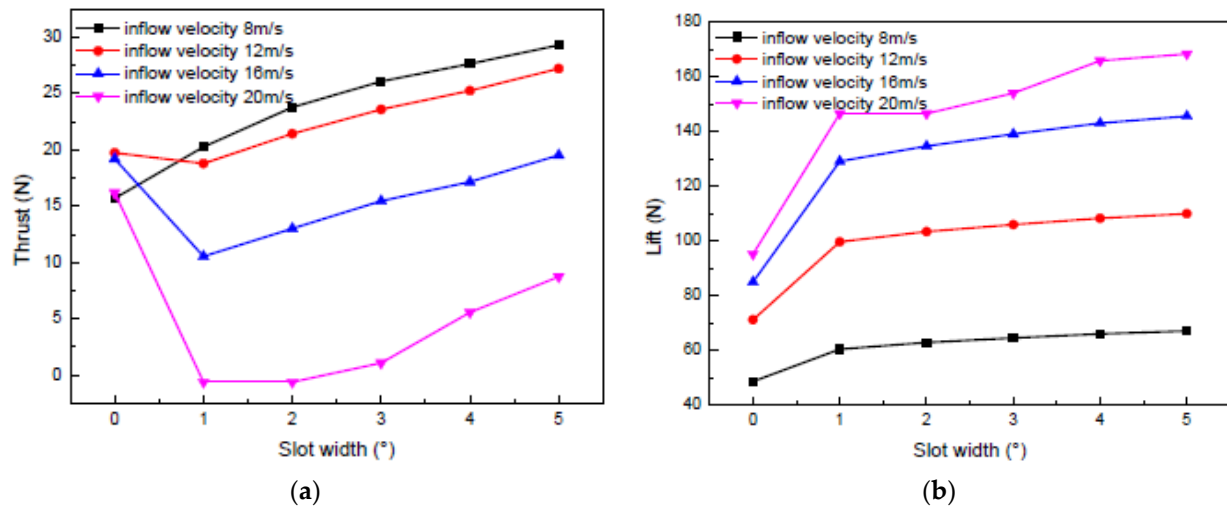


Figure 19. Distribution of wing static pressure when slot width is  $0^\circ$ ,  $1^\circ$  and  $5^\circ$ .

As shown in Figure 20, as the inflow velocity increases, the thrust gradually decreases, and the lift gradually increases. After slotting, the thrust gradually increases with the increase in slot width when the inflow velocity is small. When the inflow is large, the thrust first decreases and then increases, and the lift gradually increases with the increase in slot width. The increase in lift and thrust is relatively stable and has a relatively small amplitude. Therefore, in the following analysis, a slot width of  $2^\circ$  has been selected.



**Figure 20.** The effect of slot size on lift and thrust: (a) thrust; (b) lift.

#### 3.4.2. Effect of Number of Slots on the Aerodynamic Performance of the Fan Wing

The calculation state is inflow of 8 m/s, the angle of attack of  $0^\circ$ , and the cross-flow fan rotation speed is 2000 rpm. Comparing the pressure cloud and streamline diagrams of a single slot, double slot, and no slot in Figure 21, it can be seen that the cross-flow fan has an increased impact on the incoming flow after slot opening, further changing the angle at which the incoming flow enters the cross-flow fan. After slotting, the internal pressure of the cross-flow fan decreases. After increasing the number of slots, more airflow enters the cross-flow fan and is accelerated by the cross-flow fan, resulting in higher velocity on the upper wing surface and lower velocity on the lower wing surface. At the same time, it also increases the influence of the cross-flow fan on the incoming flow, changes the direction of incoming flow into the cross-flow fan, and causes the leading edge stagnation point to move from the leading edge to the rear edge along the lower wing surface, increasing the pressure difference between the upper and lower wing surfaces of the wing and increasing lift. Thrust is mainly generated by the pressure difference of the wing in the horizontal direction and the wake discharged by the cross-flow fan. As the number of slots increases, the flow velocity and flow rate of the cross-flow fan's exhaust wake increase, while the pressure in the curved section decreases and the leading edge stagnation point moves backward along the lower wing surface, resulting in an increase in horizontal thrust.

As shown in Figure 22, by comparing the static pressure distribution on the wing surface with the reference model, it can be found that the pressure on the lower wing surface remains almost unchanged after slotting, while the static pressure on the inclined section of the upper wing surface slightly decreases, and the internal surface pressure on the leading edge curved section decreases more. Compared with Figure 21, it can be found that the pressure drop here is due to the stagnation point of the wing leading edge velocity moving along the curved section from the leading edge to the rear edge, resulting in a rapid increase in the pressure difference between the upper and lower wing surfaces. The grooving area is greatly affected by the groove, and the inner surface pressure at the grooving area of the leading edge curved section increases significantly. The inner surface pressure of the leading edge section cut by the groove decreases and the pressure difference increases after slotting.

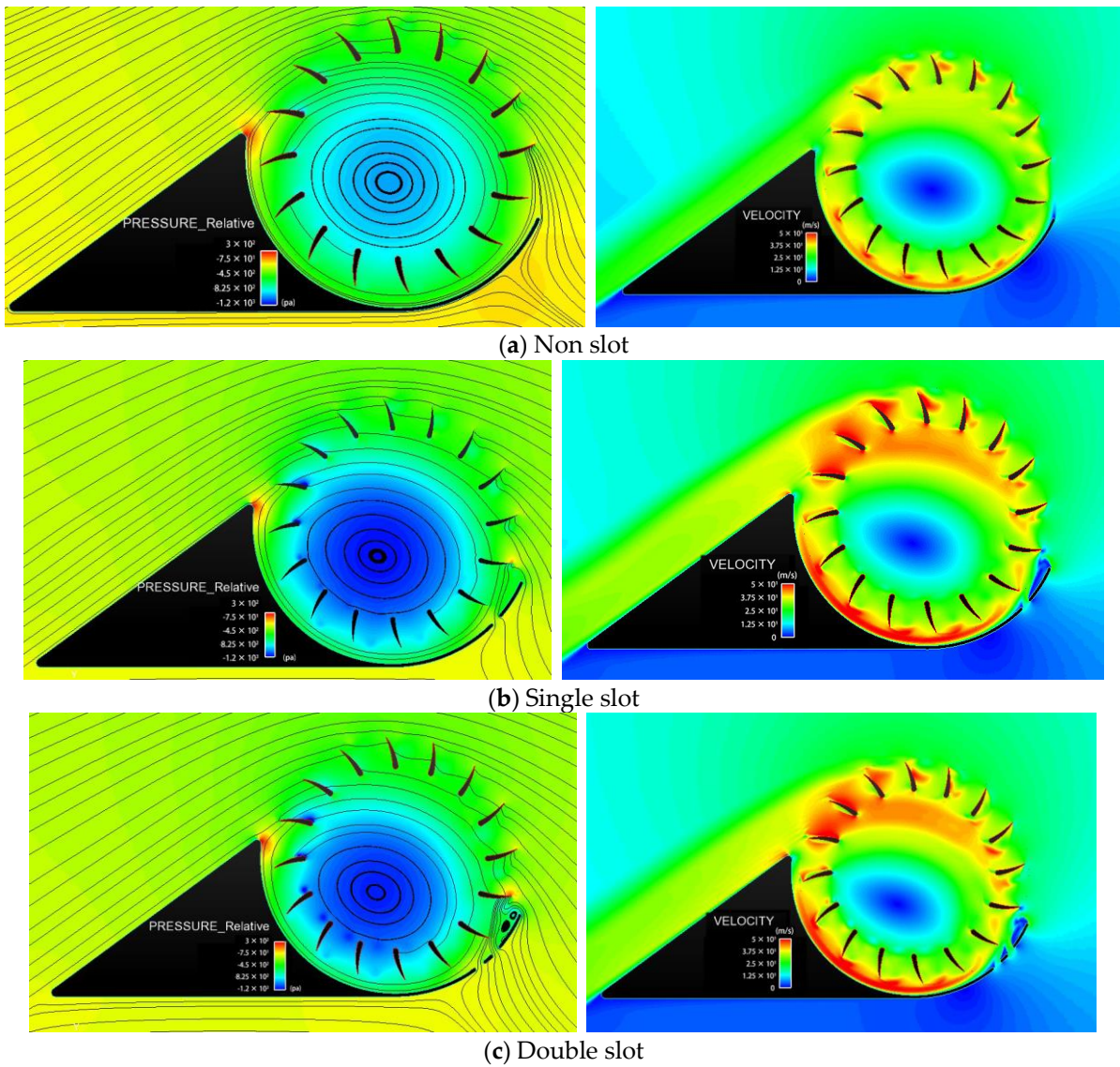


Figure 21. Flow field pressure and velocity cloud nephograms.

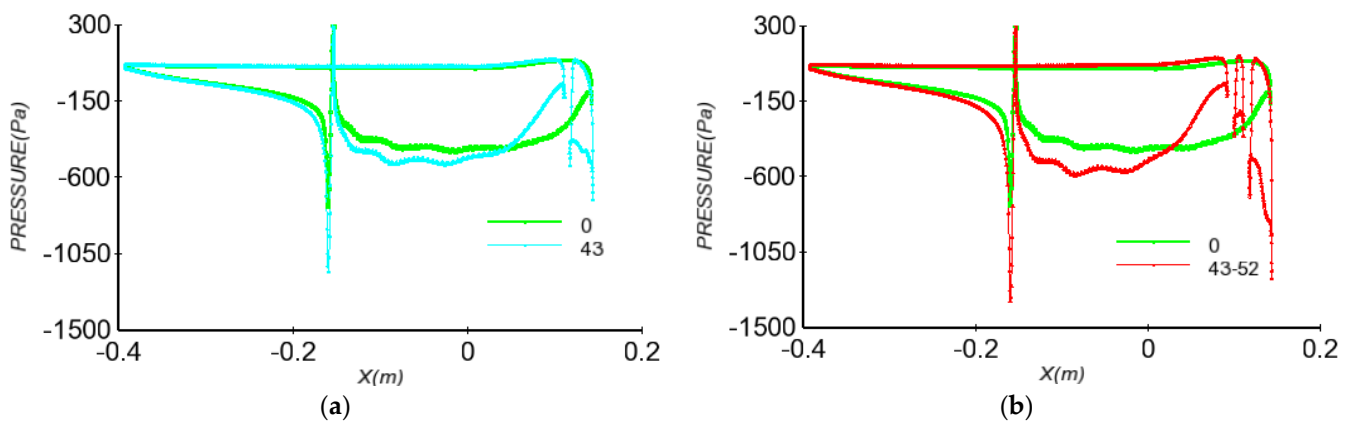


Figure 22. Comparison of static-pressure distribution on Fan Wing: (a) non slot with single slot; (b) non slot with double slot.

### 3.4.3. Effect of Slot Position on the Aerodynamic Performance of the Fan Wing

#### 1. Impact of slot position on flow field

The pressure, velocity, and streamline nephogram were numerically simulated when the incoming flow was 12 m/s, the angle of attack was 0°, and the single slot position moved from 31° to 59°. As shown in Figures 23 and 24, as the slot position moves along the lower wing surface of the leading edge arc section from the leading edge to the rear edge, the pressure in the low-pressure area of the cross-flow fan first decreases and then increases, and the flow velocity in the leading edge arc groove first increases and then decreases. Due to the influence of the rotation of the cross-flow fan on the flow field near the wing, the horizontal incoming flow will deflect near the leading edge of the wing before entering the cross flow fan. When the slot position is around 43°, the incoming flow is almost perpendicular to the slot, so more incoming flow enters the cross-flow fan. After the slot position moves to the rear edge, turbulence has already generated on the inner surface of the front edge section that has been cut by the slot. When the slot position angle is large, the negative pressure generated by turbulence causes the airflow on the inner surface of the front edge arc section to reverse (opposite to the rotation direction of the cross-flow fan).

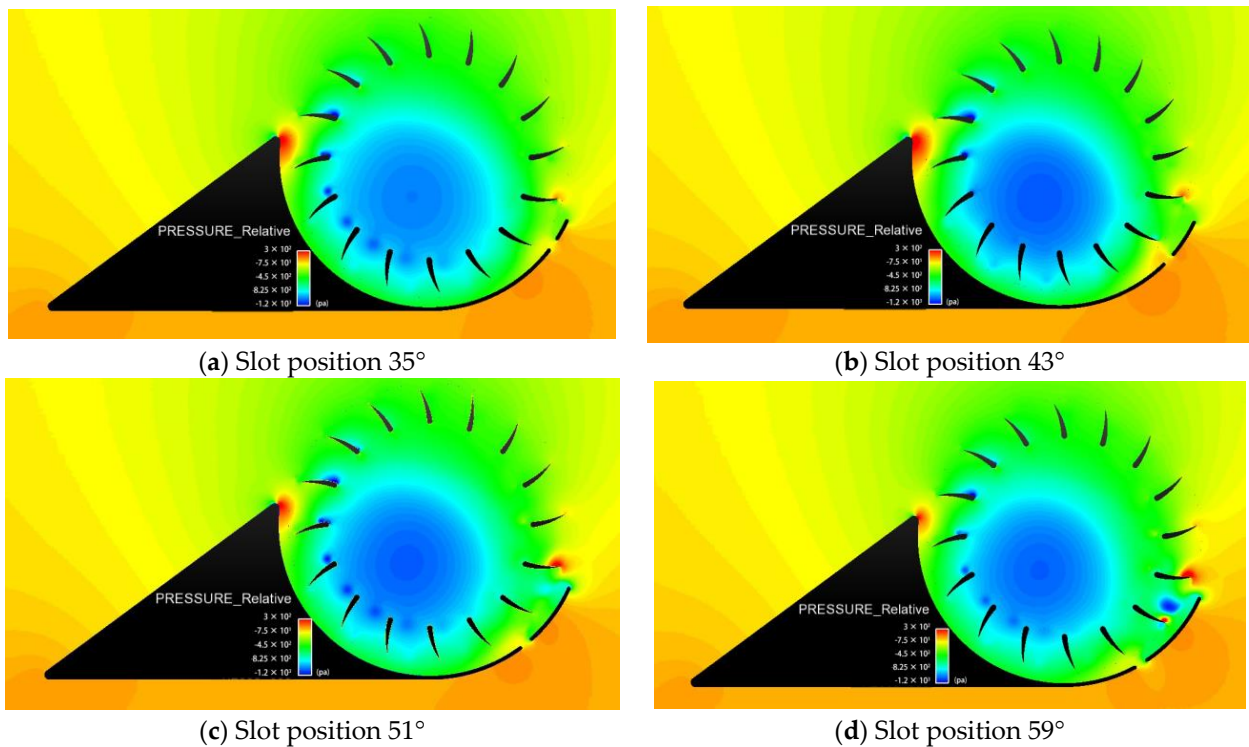


Figure 23. Pressure nephogram of Fan Wing with different single slot position.

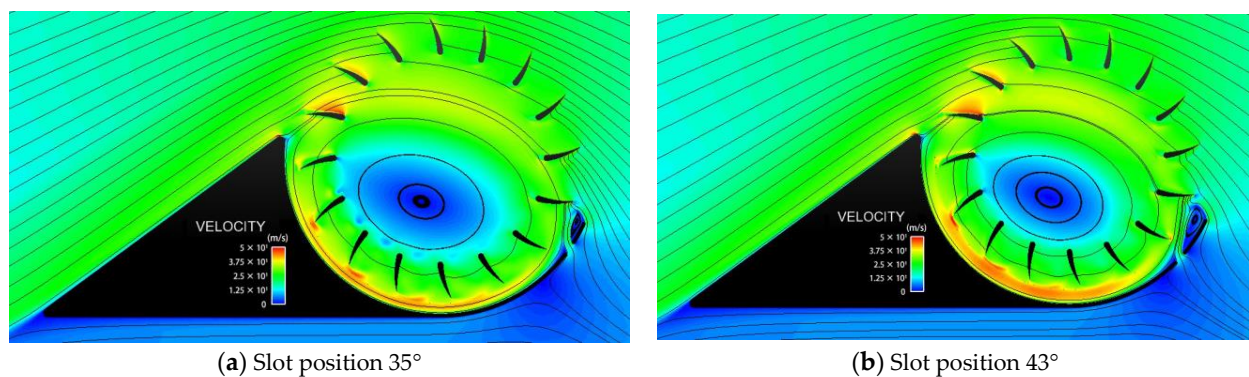
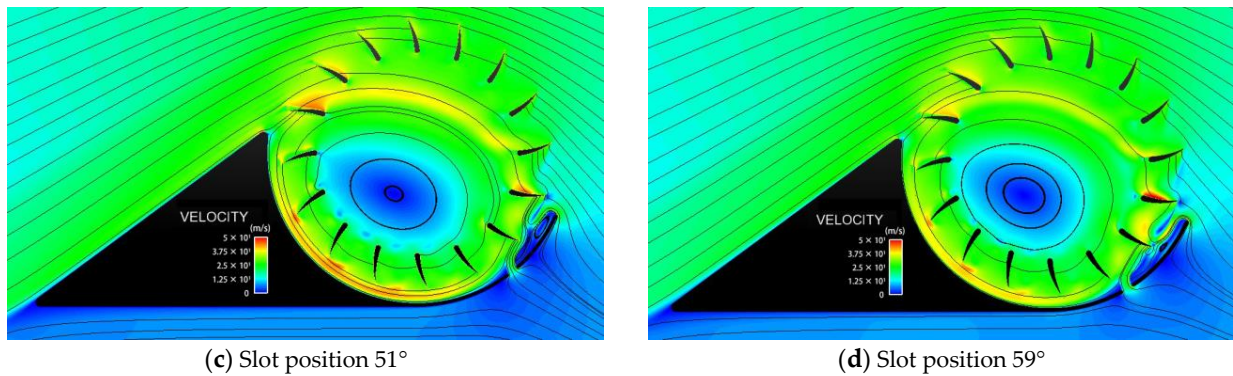
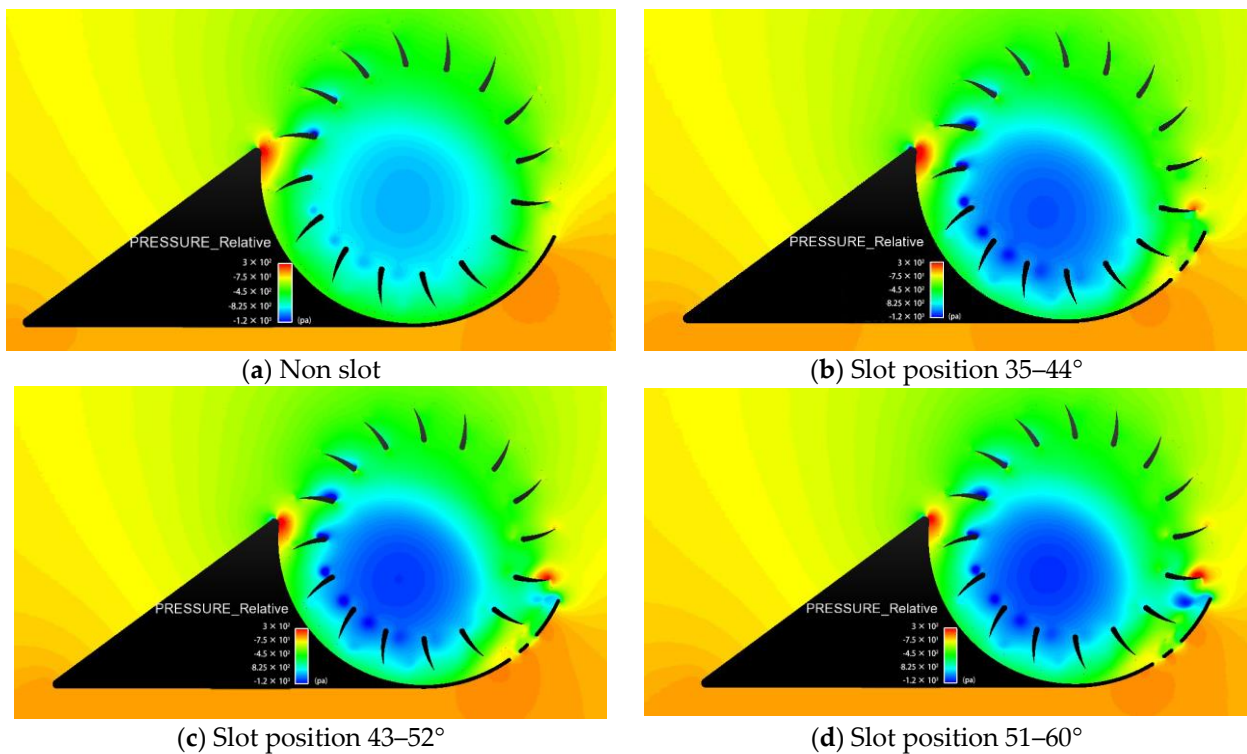


Figure 24. Cont.



**Figure 24.** Velocity and streamline nephogram of Fan Wing with different single slot position.

As shown in Figures 25 and 26, it can be seen that, after opening the double slot, more incoming flow enters the cross-flow fan. The flow velocity in the leading edge arc section increases, the low-pressure vortex pressure decreases, and the inner surface of the cut leading edge arc section also creates a turbulent zone. The pressure on the inner surface of the arc-shaped section near the slot position increases. As the slot position moves from the leading edge to the rear edge, the projection of the slot in the vertical direction gradually increases, and the affected arc-shaped section also gradually increases. This causes the positive effect of the increase in flow entering the cross-flow fan on lift and the negative effect of the destruction of the lift surface of the arc-shaped section on lift to offset each other, resulting in a phenomenon where lift first increases and then decreases.



**Figure 25.** Pressure nephogram of Fan Wing with different double slot positions.

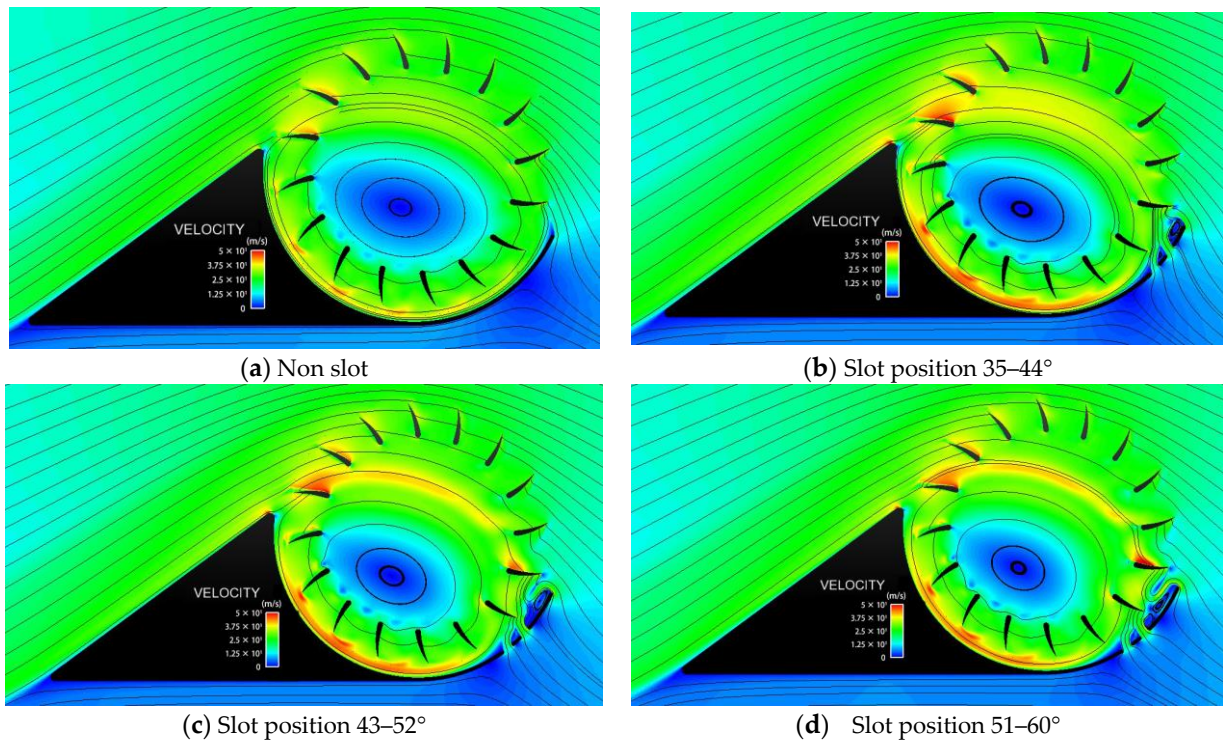


Figure 26. Velocity and streamline nephogram of Fan Wing with different double slot positions.

## 2. Impact of slot position on lift and thrust

From Figure 27, it can be seen that, when opening a single slot, as the slot position moves from the leading edge to the rear edge, the thrust first increases and then decreases. When the inflow velocity is low, the thrust after opening the slot is greater than when not opening the slot. When the inflow velocity is high, the thrust after opening the slot is smaller than when not opening the slot. The slotting position angle corresponding to the maximum thrust increases with the increase in incoming flow speed. When the inflow is 8 m/s, the thrust changes significantly with the slot position, while the slot position decreases with the increase in inflow velocity. The lift first increases and then decreases with the increase in the slotting position angle, but the increase in the lift is small. The greater the incoming flow speed, the greater the influence of the slotting position changes on the lift.

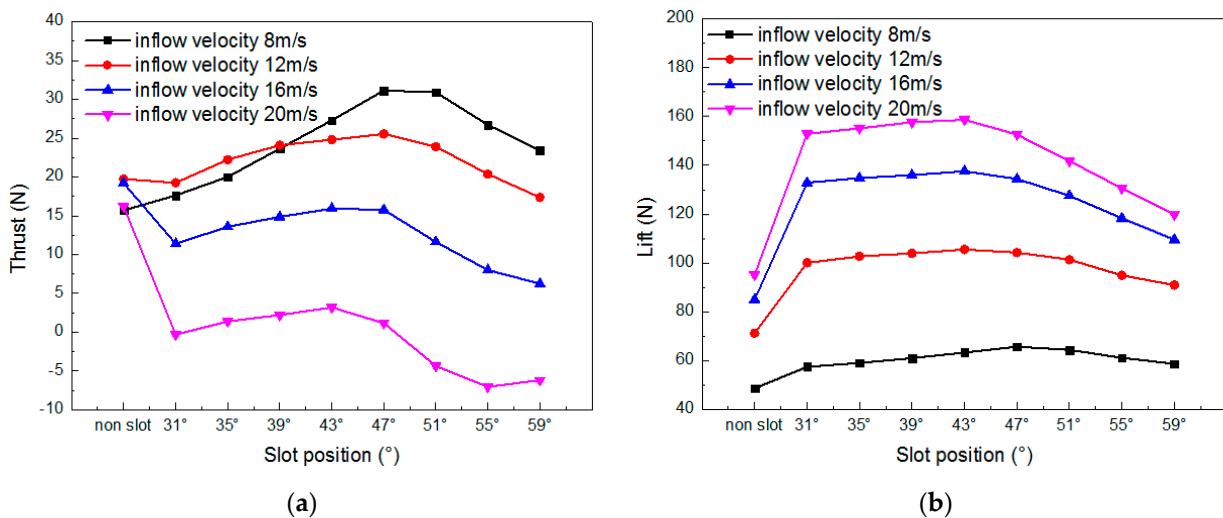


Figure 27. Force variation curve of different single slot position: (a) thrust; (b) lift.

From Figure 28, it can be seen that, as the slot position moves along the lower wing surface of the Fan Wing from the leading edge to the trailing edge, the lift and thrust first increase and then decrease at low inlet velocities. The thrust reaches its maximum value near the slot position of 37–48°, and the lift does not change much with the slot position. When the inflow velocity is high, the thrust decreases with the increase in the slotting position angle. As the inflow velocity increases, the lift increases and the thrust decreases. When the incoming flow is 8 m/s, the double groove can more than double the thrust.

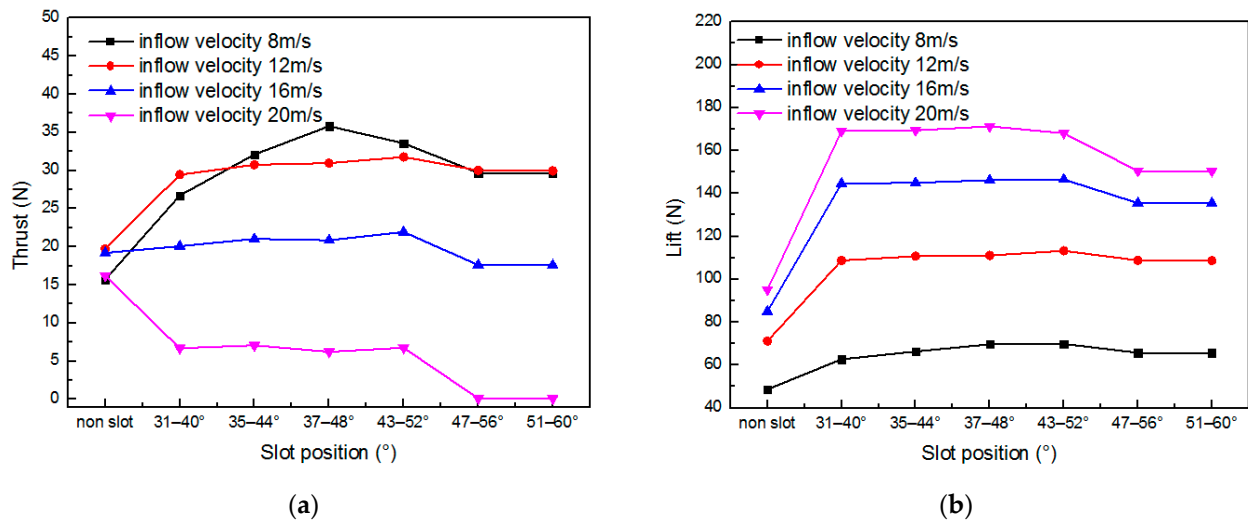


Figure 28. Force variation curves for different double slot positions: (a) thrust; (b) lift.

#### 4. Flight Test

In order to demonstrate the practicality of the designed Fan Wing, flight test validation was conducted. The size of a single Fan Wing in Figure 3b is consistent with the wind tunnel test in Figure 6b, and the Fan Wing UAV uses a total of six Fan Wings as sources of lift and thrust. A set of procedures was developed to enable rapid flight control law deployment and test on Fan Wing UAV. The flight control hardware used a Pixhawk flight computer running Ardupilot custom control algorithms firmware. In Figure 29b, it can be seen that the designed wing has flight capability. And the flight is also relatively stable.



Figure 29. Flight test of Fan Wing UAV: (a) UAV; (b) flight.

### 5. Conclusions and Further Discussion

#### 5.1. Conclusions

The factors influencing the vector force of the Fan Wing are primarily the rotation speed of the cross-flow fan, the angle of attack, and inflow velocity. It has been demonstrated that

the Fan Wing possesses characteristics such as a high angle of attack without stalling, high lift at low speeds, vertical takeoff, and a high thrust-to-weight ratio.

Slotting on the leading edge of the Fan Wing can already improve lift and thrust, and as the slot width increases, both lift and thrust will increase. The impact of opening double slots on Fan Wing lift and thrust is greater than when opening a single slot. In the case of a single slot, as the slot position moves from the leading edge to the trailing edge of the wing's lower wing surface, lift and thrust first increase and then decrease. When the inflow velocity is small, the effect of slotting on thrust was greater than on lift, while when the inflow velocity is large, the opposite is true. In the case of double slots, as the slot position moves along the lower wing surface of the Fan Wing from the leading edge to the trailing edge, the thrust first increases and then decreases when the inflow velocity is low, and decreases when the inflow velocity is high. The lift force does not change much as the slot position moves. In practical applications, the width of the slot can be controlled by the servo to achieve the goal of controlling lift and thrust.

Flight tests have demonstrated the feasibility of using the Fan Wing on aircraft.

The implication of Fan Wing research is mainly reflected in the following aspects:

- a. Improving aircraft performance: Research on Fan Wings can help improve the design and performance of aircraft, enabling them to generate lift and thrust more efficiently during flight. By optimizing the shape, size, and material of the Fan Wings, the flight speed, maneuverability, and fuel efficiency of the aircraft can be improved, thereby reducing energy consumption and environmental pollution.
- b. Enhancing aerodynamic theory: As a common aerodynamic device, Fan Wings are of great significance for the study of aerodynamic theory. By studying the aerodynamic characteristics and flow field distribution of Fan Wings, we can gain a deeper understanding of the basic principles of fluid dynamics and aerodynamics, providing a theoretical basis for the design and optimization of aircraft and other engineering fields.
- c. Promoting engineering innovation: The results of Fan Wing research can be applied to aerospace, automobile, wind power generation, and other fields, which promotes the innovation and development of engineering technology. For example, in the field of aviation, Fan Wing research can improve the takeoff and landing performance and manoeuvrability of aircraft, and improve the safety and comfort of aircraft. In the field of wind power, Fan Wing research can help optimize the design of wind turbines and improve energy efficiency.
- d. Expanding scientific knowledge: The study of Fan Wings is of great significance for deepening our understanding of scientific fields such as fluid dynamics and aerodynamics. By conducting experiments and numerical simulations on Fan Wings, complex fluid behavior and turbulence phenomena can be explored, providing new observational and experimental platforms for scientific research, and deepening the understanding of fluid motion laws in nature and engineering practice.

In summary, the significance of Fan Wing research lies in improving aircraft performance, enhancing aerodynamic theory, promoting engineering innovation, and expanding scientific knowledge. These achievements will make important contributions to the development and progress of aerospace, energy, transportation, and other fields.

## 5.2. Discussion

Through the analysis of the aerodynamic forces of the Fan Wing, it can be found that, in the case of a large installation angle, the vector force can be vertically upward (Figure 30), so that the Fan Wing UAV can also have the ability to fly vertically. However, changes in the installation angle of the Fan Wing make the structure and control of the UAV more complex. Referring to the scheme of a tandem drone, it is possible to consider placing the Fan Wings relative to each other to achieve vertical takeoff capability, as shown in Figure 31.

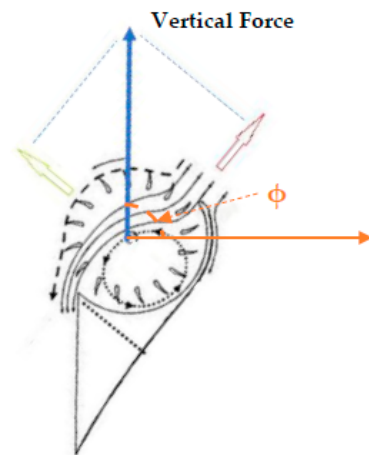


**Figure 30.** Single Fan Wing electric vertical takeoff and landing (E-VTOL) layout.

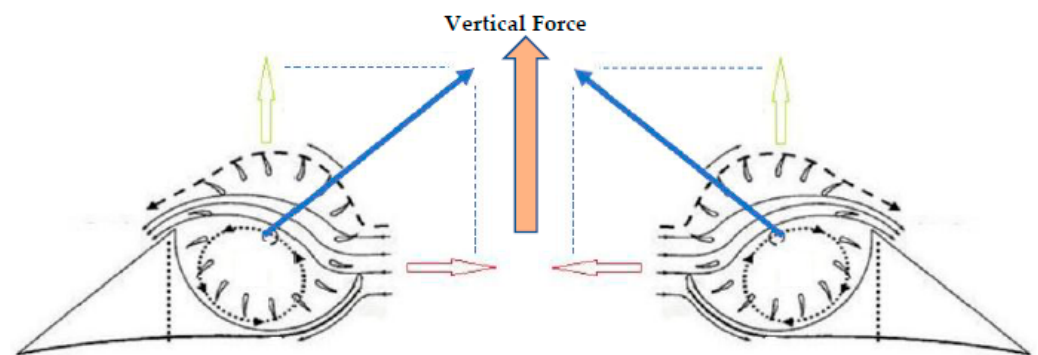


**Figure 31.** Double Fan Wing E-VTOL layout.

**Author Contributions:** Conceptualization, S.D. and Y.Z.; methodology, D.S. and Q.Z.; software, Y.Z.; validation, S.D. and Y.Z.; formal analysis, S.D.; investigation, S.D.; resources, S.D.; data curation, Y.Z. and Q.Z.; writing—original draft preparation, S.D. and Q.Z.; writing—review and editing, Y.Z.; visualization, S.D.; supervision, Y.Z.; project administration, S.D.; funding acquisition, S.D. All authors have read and agreed to the published version of the manuscript.

**Funding:** This research was funded by the National Key Laboratory of Helicopter Aeromechanics Grant No.61422201180510.

**Data Availability Statement:** The data used to support the findings of this study are available from the corresponding author upon request.

**Acknowledgments:** Thanks to Tang Zhengfei and Feng Chen for sorting out the relevant data in this paper.

**Conflicts of Interest:** The authors declare no conflict of interest.

## References

- Meng, L.; Gao, Y.; Liu, Y.Y.; Lu, S. Take-off control and characteristics of FanWing. *Aircr. Eng. Aerosp. Technol.* **2022**, *94*, 705–714. [[CrossRef](#)]
- Meng, L.; Wang, S.; Chen, Y.; Gao, Y. Emergency Flight Control Based on the Fan Wing. *Int. J. Aerosp. Eng.* **2021**, *2021*, 1216059. [[CrossRef](#)]
- Francisc, B.; Ioan, S. New Nature-Inspired Cycloidal Propeller for Low-Reynolds-Number Hovering Flight. *AIAA J.* **2019**, *57*, 2321–9653.
- Rostami, M.; Bardin, J.; Neufeld, D.; Chung, J. EVTOL Tilt-Wing Aircraft Design under Uncertainty Using a Multidisciplinary Possibilistic Approach. *Aerospace* **2023**, *10*, 718. [[CrossRef](#)]
- Saif, A.W.A.; Aliyu, A.; Dhaifallah, M.A.; Elshafei, M. Decentralized backstepping control of a quadrotor with tilted-rotor under wind gusts. *Int. J. Control. Autom. Syst.* **2018**, *16*, 2458–2472. [[CrossRef](#)]
- Altun, A.T.; Hasanzade, M.; Saldiran, E.; Guner, G.; Uzun, M.; Fremond, R.; Tang, Y.; Bhundoo, P.; Su, Y.; Xu, Y.; et al. The Development of an Advanced Air Mobility Flight Testing and Simulation Infrastructure. *Aerospace* **2023**, *10*, 712. [[CrossRef](#)]

7. Kogler, K.U. FANWING—Experimental Evaluation of an Ovel Lift & Propulsion Device. Master’s Thesis, Aeronautical Engineering Department, Imperial College, London, UK, 2002.
8. Peebles, P. Aerodynamic Lift Generating Device. US Patent 527229, 4 March 2003.
9. Seyfang, G.R. Fanwing—Developments and Applications. In Proceedings of the 28th Congress of International Council of the Aeronautical Sciences, ICAS, Brisbane, Australia, 23–28 September 2012; pp. 1–9.
10. Seyfang, G.R. Recent Developments of the Fan-Wing Aircraft. In Proceedings of the International Conference of the European Aerospace Societies, CEAS, Venice, Italy, 25 October 2011; pp. 1–7.
11. Foreshaw, S. *Wind Tunnel Investigation of the New Fan-Wing Design*; Imperial College: London, UK, 1999.
12. Bayindir, H.S.; Guillermo, P. Analysis of the Flow Field around the Wing Section of a FanWing Aircraft under Various Flow Conditions. In Proceedings of the 53rd AIAA Aerospace Sciences Meeting, AIAA, Kissimmee, FL, USA, 5–9 January 2015; p. 1936.
13. Askari, S.; Shojaeefard, M.H. Numerical Simulation of Flow an Airfoil with a Cross Flow Fan as a Lift Generating Member in a New Aircraft Model. *Aircr. Eng. Aerosp. Technol.* **2009**, *81*, 59–64. [[CrossRef](#)]
14. Askari, S.; Shojaeefard, M.H.; Goudarzi, K. Experimental Study of Stall in an Airfoil with Forced Airflow Provided by an Integrated Cross-flow Fan. *Proc. Inst. Mech. Eng. Part G J. Aerosp. Eng.* **2011**, *225*, 97–104. [[CrossRef](#)]
15. Shojaeefard, M.H.; Askari, S. Experimental and Numerical Study of the flap application an Airfoil in Combination with a Cross Flow Fan. *Int. J. Numer. Methods Heat Fluid Flow* **2012**, *22*, 742–763. [[CrossRef](#)]
16. Askari, S.; Shojaeefard, M.H. Shape Optimization of the Airfoil Comprising a Cross Flow Fan. *Aircr. Eng. Aerosp. Technol.* **2009**, *81*, 407–415. [[CrossRef](#)]
17. Duddempudi, D.; Yao, Y.; Edmondson, D.; Yao, J.; Curley, A. Computational study of flow over generic fan-wing airfoil. *Aircr. Eng. Aerosp. Technol.* **2007**, *79*, 238–244. [[CrossRef](#)]
18. Dang, T.Q.; Bushnell, P.R. Aerodynamic of Cross-flow Fans and their Application to Aircraft Propulsion and Flow Control. *Prog. Aerosp. Sci.* **2008**, *45*, 1–29. [[CrossRef](#)]
19. Kummer, J.D.; Dang, T.Q. Hight-lift Propulsive with Integrated Cross Flow Fan. *J. Aircr.* **2006**, *43*, 1059–1068. [[CrossRef](#)]
20. Du, S.; Tang, Z. The aerodynamic behavioral study of tandem Fan Wing configuration. *Int. J. Aerosp. Eng.* **2018**, *2018*, 1594570. [[CrossRef](#)]
21. Du, S.; Zhao, Q.; Wang, B. Research on Distributed Jet Blowing Wing Based on the Principle of Fan-Wing Vortex-Induced Lift and Thrust. *Int. J. Aerosp. Eng.* **2019**, *2019*, 7561856. [[CrossRef](#)]
22. Du, S.; Zhao, Q.; Tang, Z. Numerical Simulation of the Effect of Different Number Leading Edge Winglets on the Fan-Wing Aerodynamic Characteristics. *Int. J. Aerosp. Eng.* **2020**, *2020*, 8941453. [[CrossRef](#)]

**Disclaimer/Publisher’s Note:** The statements, opinions and data contained in all publications are solely those of the individual author(s) and contributor(s) and not of MDPI and/or the editor(s). MDPI and/or the editor(s) disclaim responsibility for any injury to people or property resulting from any ideas, methods, instructions or products referred to in the content.